Transverse momentum dependent multiplicities of unidentified hadrons from 2006 data

N. Makke[a,α], M. Stolarski[b], A. Martin[a],
Y. Bedfer[c], F. Bradamante[a], A. Bressan[a], E.M. Kabuss[d], F. Thibaud[c]

[a] *INFN/University of Trieste*
[α] *International Center for Theoretical Physics (ICTP)*
[b] *LIP, Lisbon*
[c] *IRFU/SPhN CEA/Saclay*
[d] *Johannes Gutenberg Universitaet, MAINZ*

Contents

1 Introduction and Motivation

Hadron production in hard scattering reactions encodes details about the hadronisation mechanism, in which quarks and anti-quarks are combined into bound states (hadrons) observed in the final state of the considered reaction. Recently a significant amount of effort has been dedicated to achieve a higher level of understanding of this mechanism and a precise determination of the fragmentation functions, as these functions represent a key ingredient in the extraction of many physics properties and in understanding some phenomena. In the COMPASS physics case, they are essential to precisely determine the nucleon longitudinal and transverse spin related distribution functions. In parallel, the transverse momentum structure of the nucleon is receiving an important amount of interest and a huge effort is being dedicated to determine with a reasonable precision the unpolarised TMDs, i.e. the Transverse Momentum Dependent parton densities (TMD-PDFs) and fragmentation functions (TMD-FFs). In the framework of the TMD factorisation scheme [1], the Semi-Inclusive DIS (SIDIS) cross section can be written as a convolution of TMD-PDFs and TMD-FFs and known elementary interactions.

Among many hard scattering reactions, semi-inclusive DIS represents a suitable tool to determine the unpolarised TMDs, which can be assessed by measuring the hadron yields normalised to the yields of DIS interactions which is referred to as multiplicities of hadrons, defined for each specific type and charge of hadrons. While the study of the z dependence of the hadron multiplicities is sensitive to the hadronisation in the collinear framework, the dependence upon the transverse momentum of the final hadron (p_T) allows to access the transverse structure of the nucleon and the formation of hadrons with a non-zero transverse momentum. This latter is generated, in the $\gamma^* - p$ c.m. frame, by the intrinsic transverse momentum of quark ($k_\perp$) and by the transverse momentum of the final hadron with respect to the fragmenting quark ($p_\perp$).

$$\frac{d^4 M^h(x, Q^2, z, p_T^2)}{dx dQ^2 dz dp_T^2} = \frac{1}{d^2\sigma^{DIS}(x, Q2)/dx dQ^2} \frac{d^4\sigma(x, Q^2, z, p_T^2)}{dx dQ^2 dz dp_T^2} \tag{1}$$

$$= \frac{\sum_q e_q^2 f_{q/p}(x, k_\perp, Q^2) D_{h/q}(z, p_\perp, Q^2)}{\sum_q e_q^2 f_{q/p}(x, k_\perp, Q^2)} \tag{2}$$

A recent fit [1] to the existing data sets, including COMPASS data [2], has been performed assuming a Gaussian parameterisation for TMDs. The fit to the COMPASS data set has shown that the approximation used is not suitable to extract the TMDs, and the shape of the data can not be reproduced.

2 History of TMD-Multiplicity studies

A first analysis of transverse momentum dependent distributions of unidentified hadrons has been performed using COMPASS data collected in 2004. The analysis [3] was performed using two-dimensional acceptance correction and covered a wide kinematic range. The final results were produced in simultaneous binning in x, Q^2, z and p_T^2, resulting in 5385 experimental points, recently published in [2].

A new analysis of transverse momentum dependent hadron multiplicities based on a data set collected in 2006 has been performed for unidentified hadrons ($h^\pm$). The choice of the 2006 data set is much advantageous than 2004 one for many reasons. First of all, the target magnet was different between the two years providing a larger angular acceptance in 2006, allowing to extend the kinematic range of possible measurements to larger x and Q^2. In addition, the new analysis extends the p_T^2 range up to 3 (GeV/c)^2 instead of 1 (GeV/c)^2, allowing a better understanding of the transverse momentum dependence of PDFs and FFs. Finally, the most important modification is in the RICH upgrade, needed for particle identification, where the central part was totally refurbished by replacing the MWPC with multi-anode photomultipliers. In the outer part, the MWPC front-end electronics were also renewed (APV instead of Gassiplex chip). As a consequence, the efficiency for pion and kaon identification increased significantly and the contamination of pion sample by kaons and vice versa is well reduced. This last point is not yet considered in the present analysis as only unidentified hadrons are considered.

A first analysis based on the 2006 data set was performed using the same binning as in the publication [2]. Only part of the results were released in June 2014 [4] and shown at the Transversity 2014 workshop. A new analysis is presented in this note, with some modifications with respect to the release in June [4]. First, the analysis uses a new binning in x and Q^2, which is chosen based on a study [5] performed to optimise the experimental kinematic coverage with the available statistics. This binning is common for all transverse spin and transverse momentum multi-dimensional analyses. At second a new Monte Carlo sample, in which the target position is corrected and the FLUKA model (instead of GHEISHA) is used to describe hadron shower, is used for the evaluation of the acceptance correction factors. More details can be found in [6].

3 Data Analysis

The analysis is based on the data set collected in 2006 using a 160 GeV/c muon beam and a lithium deutered (^{6}LiD) target longitudinally polarised. For this analysis, data taken with both polarisations of the target are combined.
Hadron multiplicities are extracted through two main steps. First the multiplicities are evaluated from raw data, corrected (in x and y) for radiative effects and then corrected for acceptance effects, which take into account the limited angular acceptance of the spectrometer. In all steps, the analysis is performed simultaneously versus x, Q^2, z and p_T^2. The choice of the (x,Q^2) binning is chosen to optimise the kinematic domain experimentally covered and the available statistics [5]. The p_T^2 binning is chosen based on a study of the experimental resolution in p_T^2, resulting in 31 bins covering the range [0,3] (GeV/c)^2. Finally 4 z bins are selected covering small, intermediate and large z ranges, see Tab. 1.

Table 1: Binning in the kinematic variables x, Q^2, z and p_T^2.

bin n.	1	2	3	4	5	6	7	8	9	10
Q^2	1.000	1.700	3.000	7.000	16.00	81.00				
x_B	0.003	0.008	0.013	0.020	0.032	0.055	0.1	0.21	0.4	0.7
z	0.200	0.300	0.400	0.600	0.800					
p_T^2	0.020	0.040	0.060	0.080	0.100	0.120	0.140	0.170	0.196	0.230
	0.270	0.300	0.350	0.400	0.460	0.520	0.600	0.680	0.760	0.870
	1.000	1.120	1.240	1.380	1.520	1.680	1.850	2.050	2.350	2.650
	3.000									

In the following are described the experimental definition of a hadron multiplicity (3.1), the data sample (3.2) used in the analysis, the kinematic selection (3.3), the selection of DIS reactions and hadron tracks (3.4) and finally the method used for the evaluation of the acceptance correction factors (3.6).

3.1 Hadron Multiplicity definition

The hadron multiplicity (for a given hadron type and charge) is experimentally defined as the averaged number of hadrons produced per deep-inelastic scattering reaction. In other terms, it is defined by the number of hadrons (N^h) retained from a selected DIS reactions sample normalised by the number of events (N^{DIS}) in this sample, evaluated in bins of the relevant kinematic variables, i.e. (x, Q^2, z, P_T^2). While the z variable is relevant to study the hadronisation mechanism, the transverse momentum of the final hadron p_T is crucial because of its relation to the transverse momentum of the quark in the target proton ($k_\perp$) and to the transverse momentum of the final hadron with respect to the fragmenting quark ($p_\perp$). The multiplicity is expressed in terms of the inclusive (σ^{DIS}) and semi-inclusive (σ^h) cross sections (Eq. 3). Evaluated from experimental data, it is limited by the geometric/angular acceptance of the apparatus and detectors efficiencies, which are taken into account in the acceptance correction factors 3.6, and biased by radiative effects which are corrected for as explained in sec. 3.7.

$$\mathrm{M^{h^\pm}(x, Q^2, z, p_T^2)} = \left(\frac{\mathrm{d^2\sigma^{DIS}}}{\mathrm{dxdQ^2}}\right)^{-1} \cdot \frac{\mathrm{d^4\sigma^{h^\pm}}}{\mathrm{dxdQ^2dzdp_T^2}} \approx \frac{\mathrm{N^{h^\pm}(x, Q^2, z, p_T^2)}}{\mathrm{N^{DIS}(x, Q^2)}} \tag{3}$$

3.2 Experimental data sample

In 2006, 13 weeks of data have been collected in total. However, the first part of 2006 data taking has been discarded in the analysis because of alignment issues and unstable data taking conditions (more details can be found in [7]). As a consequence, only six weeks are used in the present analysis, which yields reasonably sufficient statistics, spanning a variety of data taking conditions (which remain stable) and providing different data subsets compatible with each others. They are: 06W40 slot2 (52565-52931), 06W41slot2 (52959-53231), 06W42 slot2 (53347-53468), 06W43 slot2 (53534-53760), 06W45 slot2 (54126-54356) and 06W42 slot3 (54507-54663).

3.3 Kinematic selection

The kinematic range of the DIS event sample satisfy the conditions $Q^2 > 1$ (GeV/c)^2 and $W > 5$ GeV/c, which respectively select the deep-inelastic scattering (DIS) regime and suppress the region of nucleon resonances. The range of the fractional energy transfer to the virtual photon $0.1 < y < 0.9$ excludes the region where the momentum resolution starts to degrade (lower limit) and the kinematic region where large radiative corrections to inclusive cross section are required (upper limit). An equivalent cut on the hadronic final-state system $W > 5$ GeV/c is applied. Finally only events recorded by one of the inclusive triggers, Outer Trigger (OT) or inclusive Middle Trigger (iMT), are selected in the range $0.004 < x < 0.7$. In addition to these kinematic requirements, some geometrical cuts are applied, for example to ensure that the interaction vertex lie inside the target material. These cuts are listed in sec. 3.4.

The hadron candidates in the retained DIS events are subject to further cuts. First of all, hadron tracks must have traversed less than 15 radiation lengths before being detected in a racking detector to ensure that they are not identified as muons. In addition, hadron tracks must have hits in tracking detectors placed before and after the SM1 magnet, and must not cross the SM2 yoke. Hadron fractional energy z is constrained to the range [0.2, 0.8]. The lower cut is applied to select the current fragmentation regime. The upper cut is to exclude the kinematic domain where the contribution from diffractive production mechanisms is significantly important (up to 40% in hadron yields). The full list of cuts applied on DIS events and hadrons is presented in the next section.

3.4 Event and hadron selection

The following selection criteria are applied to the sample of events recorded in the selected weeks and final stare hadrons in the retained events. The effect of each cut on the statistic of DIS events is given in Tab. 2, where a more detailed table showing the statistics of DIS events, positive and negative hadrons for each week used in the analysis is also shown (included in the note for documentation).

3.4.1 DIS selection

Only DIS interactions with following requirements are selected

1. DIS event with BestPrimaryVertex
2. DIS event with reconstructed muon (Phast routine PaVertex::iMuPrim())
3. The beam muon must have momenta between 140 GeV/c and 180 GeV/c.
4. The reconstructed vertex of the primary interaction should lie in the target material.
5. A more restricted range in the Z coordinate of the primary interaction vertex, i.e. ([-56 cm,-35 cm] $\cup$ [-20 cm,31 cm] $\cup$ [43 cm,66 cm]), is required to remove events which do not lie in the fiducial target volume because of the non-perfect description of the target in MC.
6. The extrapolated beam tracks are required to fully cross both target cells (R<1.4cm, Y<1.4cm). This cut is applied for consistency with the cuts applied for asymmetry measurement.
7. Photon virtuality: $Q^2 > 1$ (GeV/c)^2
8. Lepton energy fraction transferred to the virtual photon: $y \in [0.1, 0.9]$
9. centre of mass energy for final state hadrons: $W \in [5\text{ GeV/c}, 17\text{ GeV/c}]$
10. BMS cut which eliminates badly reconstructed beam track (using PaParticle::Chi2CutFlag())
11. Inclusive triggers (Outer Trigger & Inclusive Middle Trigger)

3.4.2 Hadron selection

All outgoing particles in the retained DIS interaction vertices are hadron candidates and are subject to the following criteria

1. Particle is not identified as muon in Phast
2. The Z coordinate of the first measured hit is upstream of SM1 ($Z_{first} < 400$cm)
3. The Z coordinate of the last measured hit is downstream of SM1 ($Z_{last} > 400$cm)
4. hadron track do not passes through the SM2 yoke (PaTrack::CrossYokeSM2())
5. Hadron tracks must have traversed less than 15 radiation lengths of material ($XX_0 < 15$)
6. Hadron energy in units of the virtual photon energy must lie in [0.2, 0.8]

DIS cuts	# events	Fraction
Total number of events	4,220,931,900	1.00
With Primary Vertex (PV)	1,385,737,276	0.33
PV with reconstructed muon	772,304,095	0.56
PV with incident muon	772,304,095	1.00
Interaction in target material	407,203,362	0.53
Beam muon crosses target cells	398,982,028	0.98
Beam energy $\in$ [140,180]	397,099,355	1.00
$Q^2 > 1$ (GeV/c)^2	39,926,910	0.10
$0.1 < y < 0.9$	27,344,501	0.69
5 (GeV) $< W <$ 17 (GeV)	27,203,903	0.99
$0.004 < x_B < 0.7$	27,180,032	1.00
BMS	21,960,977	0.81
Inclusive trigger	14,309,103	0.65
$Z_{Vtx} \in [-56, -35] \cup [-20, 31] \cup [43, 66]$	12,988,866	0.91

Cut	W40	W41	W42	W43	W45	W46
All events	898059765	703878523	711103435	803949897	664139971	439800309
Events with BPV	298609098	231319770	226630135	262255180	219063173	147859920
Events with μ'	166782370	124466227	125563908	150475968	120335900	84679722
Events with μ	166782370	124466227	125563908	150475968	120335900	84679722
InTarget()	88019225	65174512	66706849	79352164	64294985	43655627
In cells	88019209	65174497	66706782	79352096	64294947	43655602
CrossCells	86266438	63840744	65374107	77730603	63017083	42753053
E_μ	85959028	63538992	65046599	77312890	62716749	42525097
Q^2	9207779	6622004	6742922	7405618	5972216	3976371
y	6289312	4538680	4618632	5094795	4099733	2703349
W	6256125	4515412	4594986	5069214	4078585	2689581
x_B	6250532	4511452	4590947	5064781	4075039	2687281
chi^2	5175003	3636184	3667449	4017673	3330453	2134215
Trigger	3443794	2391727	2383350	2584704	2131133	1374395
in cells	3134040	2168834	2160204	2343557	1932107	1250124
hadrons						
h	9399821	6581955	6681732	7163887	5964539	3771455
h^+	4992012	3504385	3554192	3807169	3175040	2007199
h^-	4407809	3077570	3127540	3351215	2789499	1761378
$0.2 < z < 0.8$						
h	1860043	1286244	1288572	1390535	1150629	738820
h^+	1034730	715673	718403	774169	642177	411397
h^-	825313	570571	570169	616366	508452	327423

Table 2: Statistics of all selection cuts for all 2006 weeks selected for this analysis.

3.5 Final statistics

The total numbers of selected DIS interactions and final-state hadrons (h^+/h^-) are listed in Tab.3 for each of the six weeks of data selected in this analysis. The same numbers from the MC sample used in the analysis are listed in Tab.4. With the available MC sample, the number of DIS interactions reconstructed in both experimental data and MC is similar. However, for the acceptance estimation, one uses for the MC significantly larger amount of statistics with respect to the experimental data (at least factor 5 more). This amount of statistic is not yet available, but it is expected to have this factor for the foreseen publication.

Week	DIS	h^+	h^-	h^+ (0.2<z<0.8)	h^- (0.2<z<0.8)
W40	3,134,040	4,992,012	4,407,809	1,034,730	825,313
W41	2,168,834	3,504,385	3,077,570	715,673	570,571
W42	2,160,204	3,554,192	3,127,540	718,403	570,169
W43	2,343,557	3,807,169	3,351,215	774,169	616,366
W45	1,932,107	3,175,040	2,789,499	642,177	508,452
W46	1,250,124	2,007,199	1,761,378	411,397	327,423
Total	12,988,866	21,039,997	18,515,011	4,296,549	3,418,294

Table 3: Total number of DIS interactions and hadron tracks from 2006 selected data.

MC	DIS	h^+ (0.2<z<0.8)	h^- (0.2<z<0.8)
	14,746,406	5,127,934	4,070,062

Table 4: Total number of reconstructed DIS interactions and hadron tracks from 2006 MC.

3.6 Acceptance effects

The multiplicities extracted from experimental (raw) data are evaluated in a limited geometrical/angular acceptance defined by the experimental apparatus and are biased by radiative effects which affect differently the different kinematic ranges. The multiplicities must be corrected for all these effects/limitations.

The acceptance effects are evaluated using a Monte Carlo simulation that makes use of the LEPTO event generator and the JETSET package to simulate the hadronisation mechanism. At LEPTO level, deep-inelastic scattering events are generated in a wider kinematic range wider than the one selected in the analysis in order to take into account smearing effects. It is defined by: $Q^2 > 0.8$ (GeV/c)^2, $x \in [10^{-4}, 0.99]$, $y \in [0.05, 0.95]$ and $\nu \in [0, 250]$ (GeV/c), more details about the options used for the MC production can be found in [8]. For the simulation of the hadronisation mechanism the values of the parameters of the fragmentation functional form, optimized in [9] for COMPASS data, are chosen to guarantee a reasonably good description of experimental data although the acceptance does not depend on the level of agreement between experimental data and MC simulation. The produced particles are tracked using a GEANT3 model (COMGeant) of the COMPASS apparatus. The tracks are finally reconstructed with the same algorithm used for experimental data. The Monte Carlo sample contains both reconstructed and generated properties of all recorded tracks, needed in the acceptance evaluation. It consists of $\sim 106{\times}10^6$ generated DIS interactions for the yet available MC sample. Finally, for documentation, the RICH detector is not correctly simulated in this MC production. This new MC makes use of the FLUKA model for the simulation of secondary interactions in the target instead of GHEISHA, used in previous MC production (by default). The first study of the difference between the two moles GHEISHA and FLUKA was performed by C. Hoeppner for the analysis of the cross-section for high-p_T hadron production at low Q^2 and was found that the description of re-interactions using FLUKA agrees better with the COMPASS data, at very high p_T, i.e. $p_T > 1.8$. For the present analysis, the highest p_T is ~ 1.7 for which both GHEISHA and FLUKA give similar description of the secondary interactions in the target. However, to be consistent between various analyses, FLUKA is selected.

The acceptance correction factor is evaluated, for each hadron charge and in each (x,Q^2,z,p_T^2) kinematic bin, by the ratio of the number of reconstructed hadron tracks (N_r^h) to the number the generated hadrons (N_g^h), both numbers counted from the reconstructed DIS interactions sample retained by the kinematic selection, as defined in Eq. 4. Since the numbers of generated and reconstructed hadron tracks are correlated, the errors on the acceptance evaluation are calculated using Eq. 5, which is derived from an analytical calculation starting from a binomial probability function and using the Bayesian approach (more details can be found in [10]), for the case $N_r^h \leq N_g^h$ and assuming independent numbers N_r^h and N_g^h in the case $N_r^h > N_g^h$. The indices g and r refer respectively to the values of the kinematic variables evaluated for the generated and the reconstructed hadrons and muons tracks.

$$A^h(x, Q^2, z, P_T^2) = \frac{\mathrm{N_r^h(x_r, Q_r^2, z_r, P_{T,r}^2)}}{\mathrm{N_g^h(x_r, Q_r^2, z_g, P_{T,g}^2)|_{DIS_{rec}}}} \tag{4}$$

$$(\Delta A)^2 = \frac{(\mathrm{N_r^h}+1)(\mathrm{N_g^h}-\mathrm{N_r^h}+1)}{(\mathrm{N_g^h}+2)^2(\mathrm{N_g^h}+3)} \tag{5}$$

For the numbers of reconstructed DIS interactions and of reconstructed hadron tracks (numerator in Eq. 4), the same cuts as for experimental data (listed in section 3.4) are applied while for the numbers of generated hadrons (denominator in Eq. 4), cuts on kinematic variables (x, Q^2, y, W, z) are mainly applied. For completeness, the cuts applied on the MC sample are listed below:

- MC Reconstructed: Cuts defined in 3.4. (Same cuts applied on experimental data for both inclusive and semi-inclusive events are applied here).
- MC Generated: in addition to kinematic range selection
  $Q^2 > 1$ (GeV/c)^2, $W > 5$ GeV, $y \in$ [0.1,0.9], $x \in$ [0.003,0.7]
  1. Inclusive events selection:
     (a) Energy of the muon beam required in the range [140 GeV,180 GeV]
     (b) Primary interaction inside target fiducial volume, i.e.
     $Z \in [-56\text{ cm},-35\text{ cm}] \cup [-20\text{ cm},31\text{ cm}] \cup [43\text{ cm},66\text{ cm}]$.
     (c) Muon beam track crosses all target cells
  2. Semi-inclusive events selection
     (a) fractional energy $z \in$ [0.2,0.8]
     (b) Particle is not electron/positron or muon/antimuon (Lepto PID >7)

The acceptance correction factors are shown in Fig.1 for two z bins for illustration. For $z > 0.3$, the acceptance is larger than 60 % in all kinematic bins except in few (x,Q^2) bins where the acceptance decreases at large p_T^2. At low z ([0.2,0.3]), the acceptance is larger than 50% in all bins except in the largest x bin in each Q^2 bin where the acceptance decreases very rapidly vs p_T^2. In addition to these observations, the acceptance correction factors significantly fluctuate with respect to the statistical uncertainty evaluated using Eq. 5. This effect is due to the limited MC statistics.

For the bins where the acceptance decreases very rapidly, the acceptance correction factors are very large and thus the hadron multiplicities in these bins are rejected. To summarise, the considered (x,Q^2) bins for the four z bins are drawn in Tabs. 5, 6 and 7 respectively. The red bands represent bins rejected because of large acceptance corrections and the green bands represent bins rejected because of lack of statistics. Finally the gray bands represent the bins that are selected in the analysis.

3.6.1 Contribution of the electrons/positrons to the hadron sample

As previously described, the hadron tracks in both experimental data and MC are subject to the same selection criteria. Among these cuts, no cut on the ID of hadron tracks is applied because we are aiming to measure multiplicities for unidentified hadrons. However, the hadron sample is contaminated by electrons/positrons, which are present in both experimental and MC data. If the fraction of electrons/positions in the hadron sample is the same in both experimental data and MC, this effect is

Figure 1: Acceptance correction factors versus (x,Q^2,p_T^2) for positive and negative hadrons in 2 z ranges.

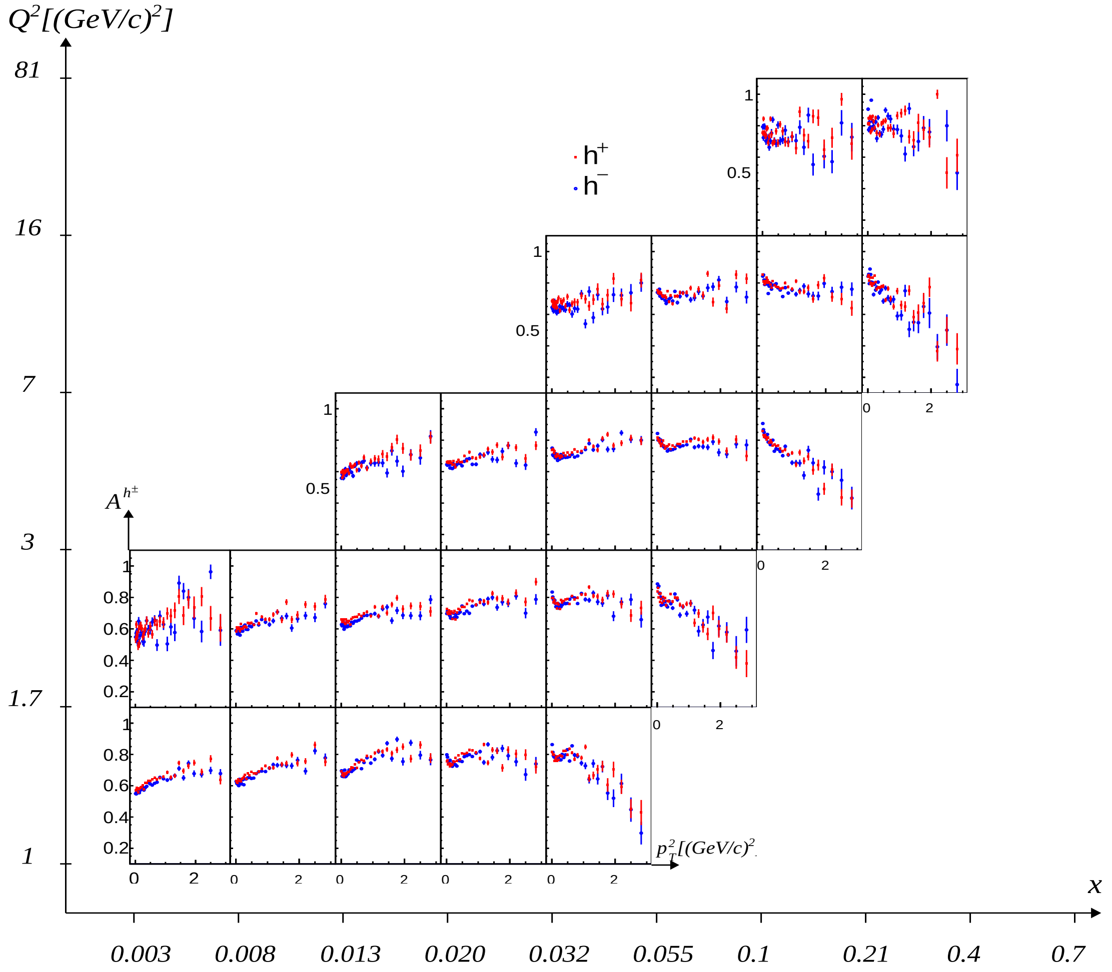

(a) $0.3 < z < 0.6$

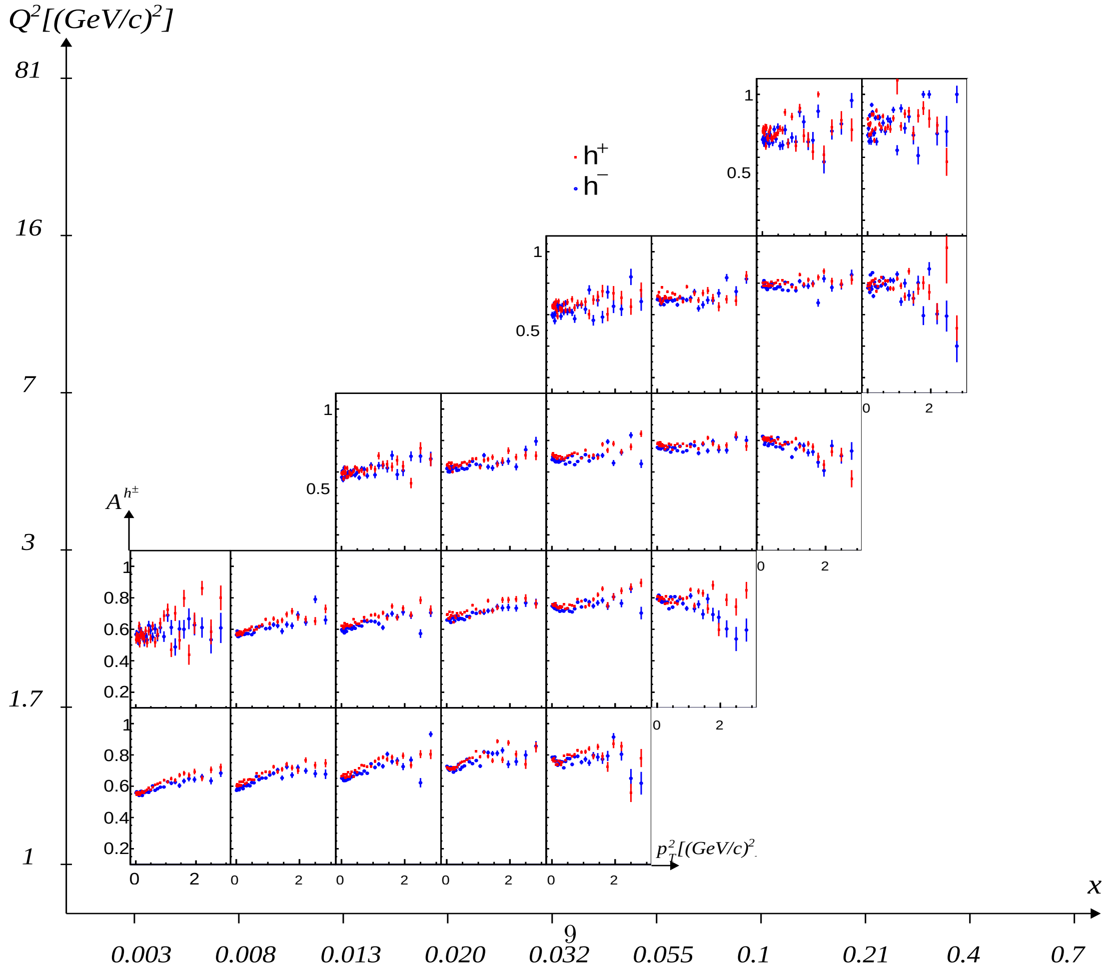

(b) $0.6 < z < 0.8$

canceled when dividing the raw multiplicities by the acceptance correction factors. This fraction has been compared between experimental and MC data sets for the momentum range ($P \in [3, 8]$ GeV) where the RICH ensures electron identification and found to be compatible on the 25% level. On the basis of this check, the MC is used to evaluate the fraction of electrons/positrons in the hadron sample in the full momentum range (covered in the present analysis). This fraction is found to be smaller than 5% for $z > 0.3$ and larger than 10 % for $z < 0.2$ and $p_T^2 < 0.1$. Thus all kinematic bins where the electron/positron fraction is larger than 5% are excluded.

Table 5: Selected (x,Q^2) bins for $z \in [0.2, 0.3]$.

Q^2/x	1	2	3	4	5	6	7	8	9
5						b_{56}	b_{57}	b_{58}	b_{59}
4				b_{44}	b_{45}	b_{46}	b_{47}	b_{48}	
3		b_{32}	b_{33}	b_{34}	b_{35}	b_{36}	b_{37}	b_{38}	
2	b_{21}	b_{22}	b_{23}	b_{24}	b_{25}	b_{26}	b_{27}		
1	b_{11}	b_{12}	b_{13}	b_{14}	b_{15}	b_{16}			

Table 6: Selected (x,Q^2) bins for $z \in [0.3, 0.6]$.

Q^2/x	1	2	3	4	5	6	7	8	9
5						b_{56}	b_{57}	b_{58}	b_{59}
4				b_{44}	b_{45}	b_{46}	b_{47}	b_{48}	
3		b_{32}	b_{33}	b_{34}	b_{35}	b_{36}	b_{37}	b_{38}	
2	b_{21}	b_{22}	b_{23}	b_{24}	b_{25}	b_{26}	b_{27}		
1	b_{11}	b_{12}	b_{13}	b_{14}	b_{15}	b_{16}			

Table 7: Selected (x,Q^2) bins for $z \in [0.6, 0.8]$.

Q^2/x	1	2	3	4	5	6	7	8	9
5						b_{56}	b_{57}	b_{58}	b_{59}
4				b_{44}	b_{45}	b_{46}	b_{47}	b_{48}	
3		b_{32}	b_{33}	b_{34}	b_{35}	b_{36}	b_{37}	b_{38}	
2	b_{21}	b_{22}	b_{23}	b_{24}	b_{25}	b_{26}	b_{27}		
1	b_{11}	b_{12}	b_{13}	b_{14}	b_{15}	b_{16}			

3.7 Radiative effects

In addition to the acceptance effects, the experimental multiplicities are affected by QED radiative effects, which introduce a systematic bias of the observed (measured) kinematics with respect to the true kinematics. The most important contributions at first order are the initial and final state radiation of a real photon by the incoming and the outgoing lepton respectively, vertex corrections and vacuum polarisation. The correction of these effects was applied to the raw data using radiative correction weights defined as:

$$\eta(x, y) = \frac{\sigma_{1\gamma}}{\sigma_{measured}}(x, y) \tag{6}$$

where $\sigma_{1\gamma}$ denotes the cross section in the one photon exchange approximation (Born level) and $\sigma_{measured}$ denotes the measured cross sections which includes radiative effects. These weight factors [13] have been evaluated for the kinematic domain covered by the SMC experiment, which is similar to the COMPASS kinematic range. They are provided in [15]. The data are also affected by radiative effects versus semi-inclusive kinematic variables, in our case, z and p_T^2. However these corrections are not applied to the data for the simple reason that no calculation exists for our kinematic range. However, a study is ongoing to study and estimate these effects using the RADGEN simulation [14].

3.8 Diffractive meson production

The hadron sample selected from the DIS events sample is contaminated by hadrons produced by the decay of vector mesons diffractively produced (DVMP for Diffractive Vector Meson Production) in lepton-nucleon scattering. The dominant channel at the COMPASS kinematics is the diffractive production of ρ^0, which is often exclusive except in 20% of the cases where an excitation and a decay of the nucleon target occur (diffractive dissociation) resulting in pion production:

$$\gamma^\star p \rightarrow \rho^0 p \rightarrow p\pi^+\pi^- \tag{7}$$

$$\gamma^\star p \rightarrow \rho^0 N^\star(\Delta) \rightarrow \pi^+\pi^- X \tag{8}$$

Since these pions cannot be distinguished from pions produced in semi-inclusive DIS, their contribution to the multiplicities can be evaluated, based on a MC study. A detailed study where an evaluation of this contribution per bin has been performed [11] for p_T-integrated multiplicities. The correction for this effect is not yet settled neither on the experimental side nor on the theoretical one, and theoreticians still use the experimental data without this correction. Thus we estimate this effect for completeness. In the present analysis, we do not correct for this effect. However for completeness, we present its size versus p_T in different z ranges and versus z in different Q^2 ranges, in Fig. 2 produced by F. Thibaud.

The contribution of hadrons from DVMP mainly affect the lowest p_T range, i.e. $p_T < 1$ and increases as z increases and Q^2 decreases. Its highest value of 40% affect the highest z ($z > 0.75$), the lowest Q^2 ($Q^2 < 2$ (GeV/c)^2) and the lowest p_T range ($p_T < 0.5$ GeV).
Finally, this contribution has been estimated in bins of x, Q^2, z and p_T^2, defined in section 3, in [14]. These factors will be used, for the foreseen publication, to provide two set of results with and without the correction for diffractive vector meson contribution.

4 systematic studies

Three systematic studies were performed for the present analysis. The first study is the stability of the experimental data (selected weeks of data taking) as a function of time by comparing the kinematic distributions of the selected DIS events and of the experimental multiplicities from different weeks. No systematic effect has been detected from this first check and consequently no systematic uncertainty is assigned.

The second study is the dependence of the acceptance corrected multiplicities on the Z coordinate of the interaction vertex inside the target material. A very detailed study [16] has been performed by evaluating the experimental multiplicities and the acceptance correction factors independently in each target cell in several combination of kinematic variables (x,Q^2,z), (x,Q^2,z) and (x,Q^2,z,P_T^2). A systematic effect has been observed between the multiplicities extracted from the upstream and downstream cells of the target which reaches up to 8-10% (maximum size of the effect). In addition, this difference was found to be y-dependent. Many studies [16] have been performed trying to understand the origin of this difference, however from all these tests there was no evidence of a particular problem with any of the target cells. In conclusion, the best choose is to consider all target cells for the evaluation of the multiplicities and to assign a conservative systematic uncertainty of 5% on the magnitudes of the multiplicities, to be applied in each bin.
A third exercise has been done to evaluate a systematic uncertainty evaluated bin by bin in order to take into account the fluctuations that appear in the final hadron multiplicities generated by the acceptance

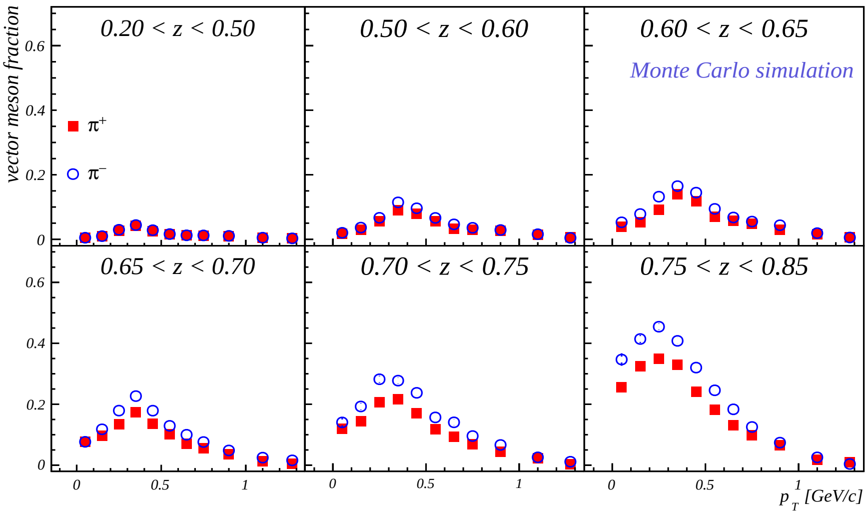

(c)

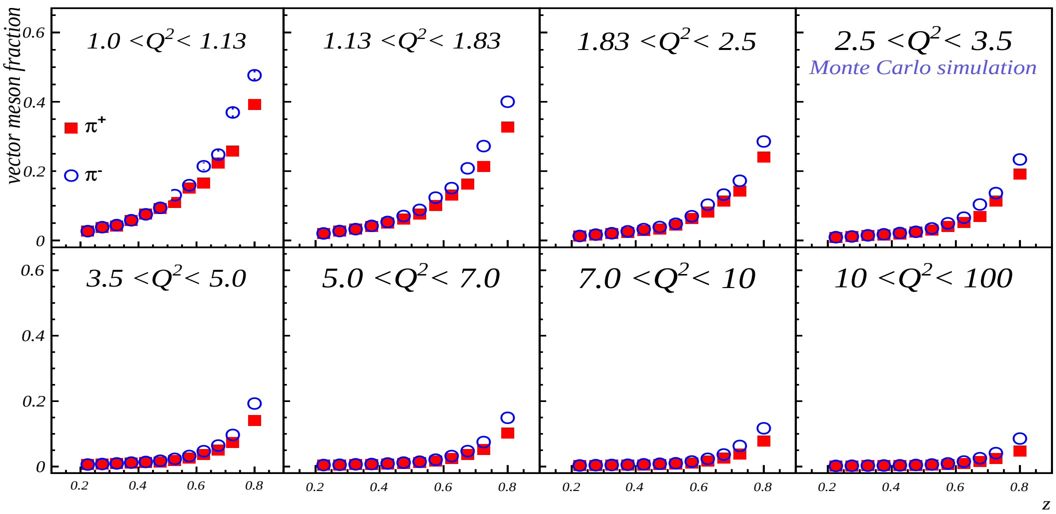

(d)

Figure 2: Fraction of pions produced by diffractive vector meson production to the total pion sample versus p_T in z bins (top) and versus z in Q^2 bins (bottom).

correction factors. Since the final multiplicities are expected to be smooth distributions, we fitted the data with a 2-exponentials function and computed the χ^2 distributions of the experimental data, for which the mean value was found to be 40 instead of the expected mean value 27. Thus a systematic error is assigned due to this effect evaluated to be $0.7.\sigma^{stat}$, evaluated per each bin.
The final systematic error applied to the final hadron multiplicities (bin by bin) are shown in Fig. 3 for all z bins, in units of the statistical uncertainties. The relative statistical uncertainties vary from 2-3 % at small p_T^2 to 10-15% at large p_T^2 ($p_T^2 > 1.8$ (GeV/c)^2) and at large x (the largest x for each Q^2 bin).

5 Results

The multiplicities corrected for radiative and acceptance effects are shown for positive and negative hadrons versus (x, Q^2, z, p_T^2) in the following figures:

- M^h(x,Q^2,p_T^2) in 4 z bins for $p_T^2 \leq 3$ (GeV/c)^2 in Fig. 5-6 –

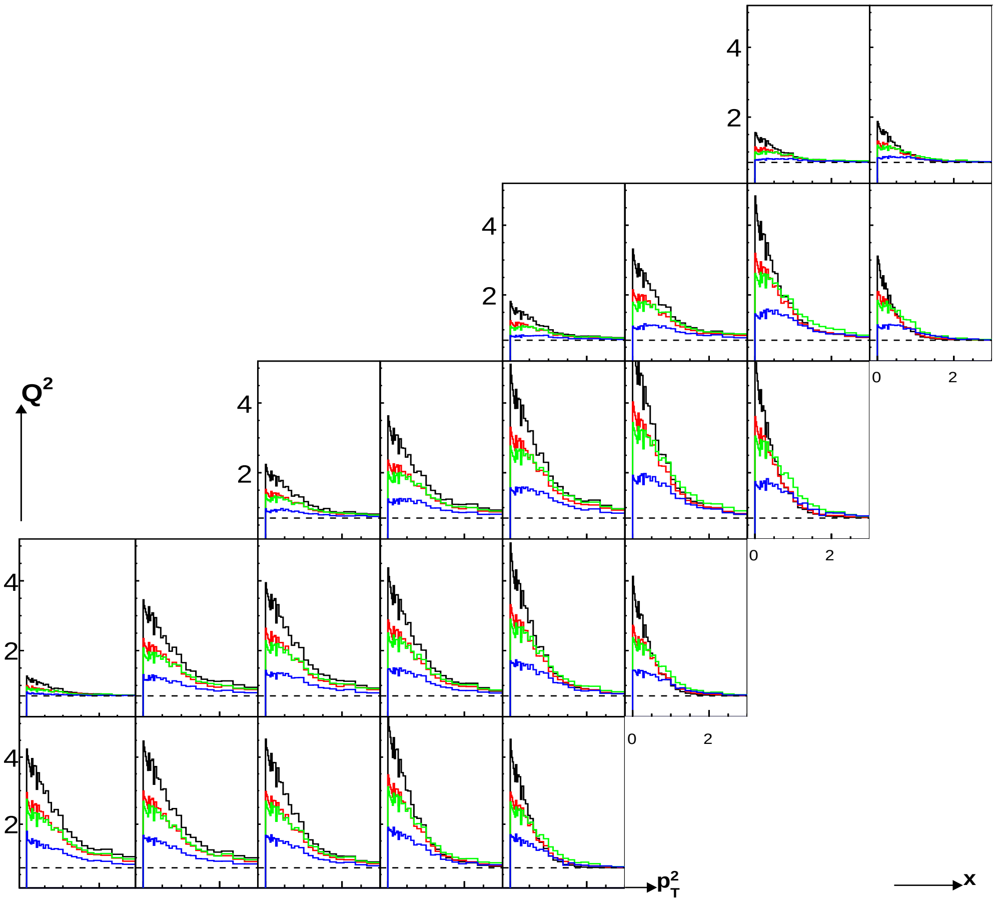

(a)

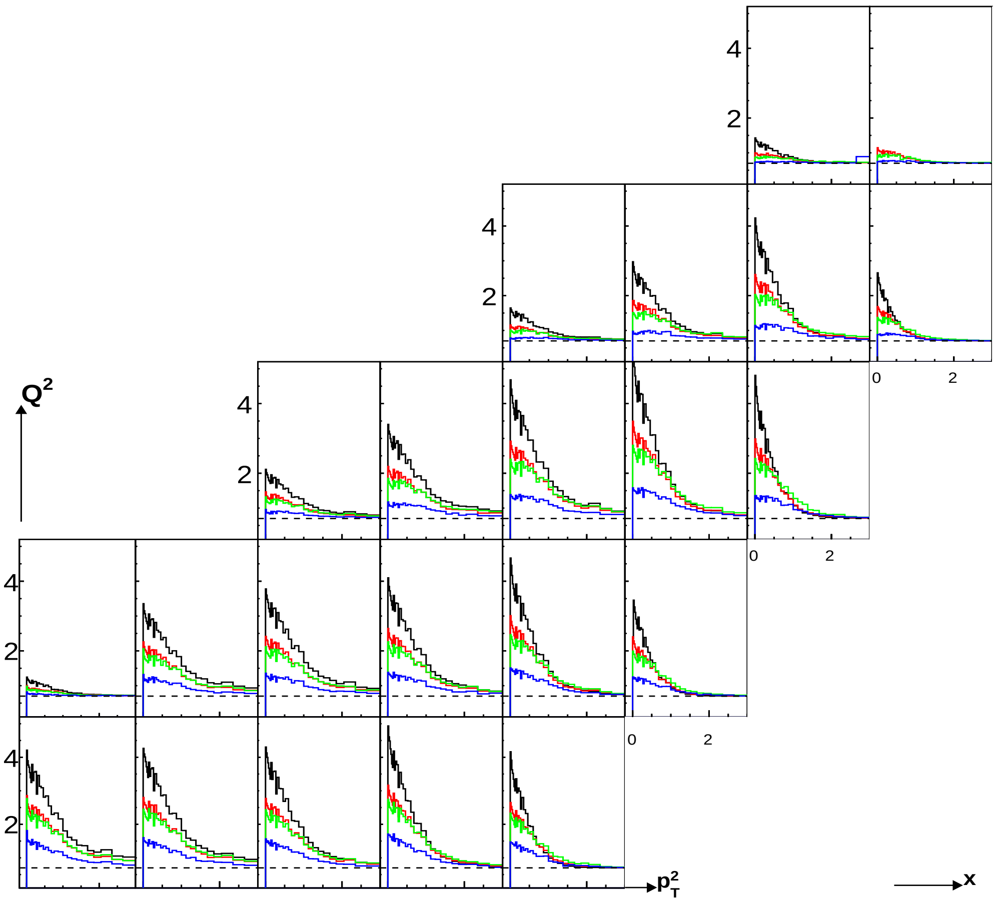

(b)

Figure 3: Systematic uncertainties in units of statistical ones versus p_T^2 in bins of x, Q^2 and z: [0.2,0.3], [0.3,0.4], [0.4,0.6], [0.6,0.8].

and with systematic uncertainty bands in Fig. 7-8

- $\mathrm{M}^h(x,Q^2,p_T^2)$ in 4 z bins for $p_T^2 \leq 1$ (GeV/c)^2 in Fig. 9-10 – and with systematic uncertainty bands in Fig. 11-12
- Ratio of multiplicities ($\mathrm{R}^h = \mathrm{M}^{h^+}/\mathrm{M}^{h^-}$) vs. (x,Q^2,p_T^2) in 4 z bins for $p_T^2 \leq 1$ (GeV/c)^2 in Fig. 13-14
- $\mathrm{M}^h(x,Q^2,z,\, p_T^2)$ in Fig. 15 vs. $(x,\, Q^2,\, z,\, p_T^2)$ (compact illustration)

In Fig. 5-6, the multiplicities are drawn versus p_T^2 in bins of $(x,\, Q^2,\, z)$ for positive (black) and negative (red) hadrons. The (x,Q^2) bins where the acceptance correction factors were found to be very large and the bins which suffer from lack of statistics are discarded. The multiplicities show a smooth p_T^2 dependence in all kinematic bins, with a difference in the magnitudes between h^+ and h^- multiplicities which becomes more pronounced as x and z increase. This observation is more evident in Fig. 9-10 where the p_T^2 range is restricted to 1 (GeV/c)^2. This observed difference is expected and is related to PDFs and FFs kinematic dependencies. At large x, the excess of h^+ is explained by the dominance of the valence quarks while at large z, it is related to the significant increase of the favored FF with respect to the unfavored FF, as illustrated in Fig. 4. A direct comparison of the magnitudes of h^+ and h^- multiplicities is illustrated in Fig. 13-14 where the ratio between h^+ and h^- multiplicities is shown versus $(x,\, Q^2,\, p_T^2)$ in the four z bins.

In Fig. 15, the multiplicities are shown in a different (compact) way, in which each panel corresponds to a given (Q^2,z) bin and where multiplicities for all x bins are drawn. The experimental data for each x bin are scaled in order to distinguish between the different x bins. In all figures, only statistical errors are shown.

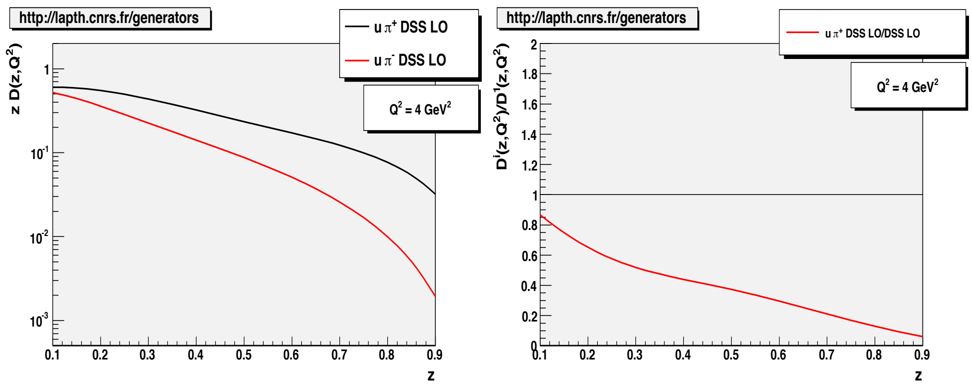

(a) (b)

Figure 4: Favored ($u \to \pi^+$ and unfavored ($u \to \pi^-$) fragmentation functions (left) from DSS parametrisation and their ratios (right) at $Q^2 = 4$ (GeV/c)^2.

6 Fits

The aim of the present analysis is to improve our understanding of the poorly known transverse momentum dependence of PDFs and FFs, and thus more focusing on the shape of the transverse momentum dependence of the experimental data. Nowadays, most of the phenomenological QCD analyses assume a Gaussian shape for both TMDs. Thus, it is interesting to check which is the function that describes at best the shape of the resulting hadron multiplicities. They were fitted with 2-exponentials function, i.e. $ae^{-\alpha p_T^2} + be^{-\beta p_T^2}$ in the range [0.01 (GeV)^2, 3 (GeV)^2], and the resulting fits are shown in:

- in Fig. 16 for $p_T^2 \leq 3$ (GeV)^2

The 2-exponentials function describe fairly well the p_T^2 dependence of h^+ and h^- multiplicities in all selected kinematic bins.

	.003-.008	.008-.013	.013-.02	.02-.032	.032-.055	.055-.1	.10-.21	.21-.4	.4-.7
$z \in$ 0.2-0.3									
81-16	-	-	-	-	-	-	1.124	1.150	-
16-7	-	-	-	-	1.612	1.125	2.686	-	-
7-3	-	-	1.770	2.135	2.086	2.420	-	-	-
3-1.7	1.107	3.536	2.428	1.854	2.342	-	-	-	-
1.7-1	2.040	2.458	2.410	1.784	-	-	-	-	-
$z \in$ 0.3-0.4									
81-16	-	-	-	-	-	-	1.650	1.406	-
16-7	-	-	-	-	1.045	1.997	1.231	1.350	-
7-3	-	-	1.558	1.792	2.279	1.529	1.379	-	-
3-1.7	1.205	1.694	2.233	3.243	2.604	1.567	-	-	-
1.7-1	2.018	2.658	2.318	2.660	3.059	-	-	-	-
$z \in$ 0.4-0.6									
81-16	-	-	-	-	-	-	1.698	2.129	-
16-7	-	-	-	-	1.179	2.249	1.100	3.096	-
7-3	-	-	1.198	1.036	1.250	1.656	1.345	-	-
3-1.7	1.547	1.467	1.224	1.825	1.906	1.498	-	-	-
1.7-1	2.788	1.558	3.510	2.800	2.725	-	-	-	-
$z \in$ 0.6-0.8									
81-16	-	-	-	-	-	-	-	-	-
16-7	-	-	-	-	2.016	1.065	2.605	0.812	-
7-3	-	-	1.533	0.935	2.162	1.307	1.076	-	-
3-1.7	-	2.186	1.748	2.262	2.986	1.814	-	-	-
1.7-1	3.693	2.590	4.040	4.748	3.193	-	-	-	-

Table 8: χ^2_{ndf} of the fit for h^+, only statistical errors are used. The χ^2_{ndf} values are shown versus (x,Q^2 ordered in the same way as for the drawn results, for the fours z bins.

	.003-.008	.008-.013	.013-.02	.02-.032	.032-.055	.055-.1	.10-.21	.21-.4	.4-.7
$z \in$ 0.2-0.3									
81-16	-	-	-	-	-	-	1.618	0.887	-
16-7	-	-	-	-	1.511	1.434	2.037	-	-
7-3	-	-	1.264	2.292	1.910	2.609	-	-	-
3-1.7	1.597	2.418	1.304	3.319	1.977	-	-	-	-
1.7-1	2.320	2.188	2.454	2.505	-	-	-	-	-
$z \in$ 0.3-0.4									
81-16	-	-	-	-	-	-	1.149	1.341	-
16-7	-	-	-	-	1.328	1.836	1.331	2.268	-
7-3	-	-	1.427	1.726	1.058	1.620	1.552	-	-
3-1.7	2.633	1.379	1.339	2.056	1.517	2.265	-	-	-
1.7-1	1.936	4.453	2.190	2.630	1.910	-	-	-	-
$z \in$ 0.4-0.6									
81-16	-	-	-	-	-	-	0.891	2.319	-
16-7	-	-	-	-	1.943	0.834	1.462	2.016	-
7-3	-	-	1.181	1.036	1.796	2.260	1.429	-	-
3-1.7	1.134	2.258	2.355	0.747	1.822	1.360	-	-	-
1.7-1	3.446	3.391	3.380	2.842	2.037	-	-	-	-
$z \in$ 0.6-0.8									
81-16	-	-	-	-	-	-	-	-	-
16-7	-	-	-	-	1.791	1.438	1.482	1.843	-
7-3	-	-	1.094	1.564	1.816	2.314	2.234	-	-
3-1.7	-	1.513	2.252	2.509	2.728	1.834	-	-	-
1.7-1	3.461	3.297	2.688	4.099	2.837	-	-	-	-

Table 9: Same as in Tab. 8 for h^-.

	.003-.008	.008-.013	.013-.02	.02-.032	.032-.055	.055-.1	.10-.21	.21-.4	.4-.7
$z \in$ 0.2-0.3									
81-16	-	-	-	-	-	-	0.551	0.554	-
16 -7	-	-	-	-	0.703	0.346	1.051	-	-
7 - 3	-	-	0.621	0.465	0.402	0.261	-	-	-
3 -1.7	0.609	0.854	0.462	0.365	0.381	-	-	-	-
1.7 -1	0.453	0.600	0.465	0.529	-	-	-	-	-
$z \in$ 0.3-0.4									
81-16	-	-	-	-	-	-	0.856	0.699	-
16-7	-	-	-	-	0.550	0.703	0.290	0.606	-
7-3	-	-	0.650	0.480	0.417	0.225	0.331	-	-
3-1.7	0.687	0.462	0.614	0.703	0.547	0.465	-	-	-
1.7-1	0.399	0.536	0.476	0.575	0.913	-	-	-	-
$z \in$ 0.4-0.6									
81-16	-	-	-	-	-	-	0.941	1.096	-
16-7	-	-	-	-	0.598	0.714	0.275	1.271	-
7-3	-	-	0.550	0.280	0.277	0.235	0.279	-	-
3-1.7	0.935	0.434	0.393	0.368	0.402	0.520	-	-	-
1.7-1	0.576	0.279	0.743	0.638	0.615	-	-	-	-
$z \in$ 0.6-0.8									
81-16	-	-	-	-	-	-	-	-	-
16-7	-	-	-	-	1.234	0.524	0.977	0.399	-
7-3	-	-	0.871	0.415	0.880	0.388	0.433	-	-
3-1.7	-	0.964	0.678	0.986	1.143	0.813	-	-	-
1.7-1	1.221	0.917	1.466	1.493	1.155	-	-	-	-

Table 10: χ^2_{ndf} of the fit for h^+, statistical & systematic errors are used. The χ^2_{ndf} values are shown versus (x,Q^2 ordered in the same way as for the drawn results, for the fours z bins.

	.003-.008	.008-.013	.013-.02	.02-.032	.032-.055	.055-.1	.10-.21	.21-.4	.4-.7
$z \in$ 0.2-0.3									
81-16	-	-	-	-	-	-	0.844	0.432	-
16-7	-	-	-	-	0.629	0.365	0.624	-	-
7-3	-	-	0.586	0.492	0.573	0.643	-	-	-
3-1.7	0.832	0.748	0.366	0.718	0.446	-	-	-	-
1.7-1	0.516	0.473	0.409	0.809	-	-	-	-	-
$z \in$ 0.3-0.4									
81-16	-	-	-	-	-	-	0.659	0.689	-
16-7	-	-	-	-	0.680	0.720	0.293	0.902	-
7-3	-	-	0.633	0.494	0.211	0.367	0.495	-	-
3-1.7	1.612	0.370	0.307	0.471	0.388	0.869	-	-	-
1.7-1	0.473	0.816	0.730	0.668	0.571	-	-	-	-
$z \in$ 0.4-0.6									
81-16	-	-	-	-	-	-	0.530	1.252	-
16-7	-	-	-	-	1.082	0.345	0.440	0.867	-
7-3	-	-	0.566	0.305	0.487	0.553	0.350	-	-
3-1.7	0.685	0.624	0.670	0.210	0.513	0.446	-	-	-
1.7-1	0.753	0.703	0.856	0.518	0.544	-	-	-	-
$z \in$ 0.6-0.8									
81-16	-	-	-	-	-	-	-	-	-
16-7	-	-	-	-	1.131	0.802	0.690	1.082	-
7-3	-	-	0.649	0.822	0.801	0.891	0.968	-	-
3-1.7	-	0.720	1.032	1.015	0.995	0.916	-	-	-
1.7-1	1.194	1.176	0.964	1.367	1.188	-	-	-	-

Table 11: Same as in Tab. 10 for h^-.

The fit was performed for two cases: using only statistical errors and using the quadratic sum of statistical and systematic errors. The obtained values of χ^2 per degree of freedom are listed in Tabs. 8-9 and 10-11 for each case respectively. Including the systematic errors which are dominating in this analysis, the χ^2 improves by at least factor 2 in all kinematic bins.
The fit slope obtained by the fit of positive and negative hadron multiplicities are also listed in Tabs. 12-13 and 14-15 for both α and β parameters respectively, using only statistical errors in the fit.

7 Conclusions

The analysis performed to extract the transverse momentum dependent multiplicities of unidentified hadrons in simultaneous bins of x, Q^2 and z is presented. The results show a smooth dependence upon p_T^2 which can be described by a function consisting of 2 exponentials. The multiplicities are different between h^+ and h^- at large x and large z, as expected from the x-dependence of the PDFs and the z-dependence of the FFs. These new results represent a new ingredient for the QCD analyses of TMDs.

8 acknowledgements

This work was partially supported by the University of Trieste, Finaziamento di Ateneo per progetti di ricerca − FRA 2012.

Table 12: First fit slope for h^+

	.003-.008	.008-.013	.013-.02	.02-.032	.032-.055	.055-.1	.10-.21	.21-.4	.4-.7
$z \in$ 0.2-0.3									
81.0-16.0	-	-	-	-	-	-	4.97±0.23	5.05±0.22	-
16.0- 7.0	-	-	-	-	4.41±0.14	4.70±0.10	5.07±0.08	-	-
7.0- 3.0	-	-	4.88±0.15	4.77±0.09	4.87±0.07	5.22±0.06	-	-	-
3.0- 1.7	4.90±0.23	5.03±0.09	5.03±0.08	5.19±0.08	5.66±0.10	-	-	-	-
1.7- 1.0	5.18±0.07	5.23±0.08	5.32±0.08	5.87±0.12	-	-	-	-	-
$z \in$ 0.3-0.4									
81.0-16.0	-	-	-	-	-	-	3.27±0.18	3.79±0.14	-
16.0- 7.0	-	-	-	-	3.52±0.18	3.44±0.07	3.95±0.07	4.42±0.12	-
7.0- 3.0	-	-	3.89±0.16	3.63±0.07	3.71±0.05	4.02±0.05	4.21±0.05	-	-
3.0- 1.7	4.57±0.42	3.93±0.09	3.83±0.06	4.19±0.07	4.35±0.07	4.29±0.08	-	-	-
1.7- 1.0	4.23±0.07	4.25±0.07	4.53±0.08	4.82±0.09	4.87±0.12	-	-	-	-
$z \in$ 0.4-0.6									
81.0-16.0	-	-	-	-	-	-	2.53±0.14	3.23±0.28	-
16.0- 7.0	-	-	-	-	2.57±0.17	2.95±0.14	3.22±0.09	3.36±0.14	-
7.0- 3.0	-	-	3.10±0.15	2.83±0.07	3.25±0.10	3.43±0.09	3.44±0.08	-	-
3.0- 1.7	4.31±0.49	3.61±0.13	3.46±0.11	3.47±0.09	3.38±0.07	3.47±0.07	-	-	-
1.7- 1.0	4.33±0.11	3.67±0.07	3.85±0.08	3.74±0.06	3.89±0.09	-	-	-	-
$z \in$ 0.6-0.8									
81.0-16.0	-	-	-	-	-	-	-	-	-
16.0- 7.0	-	-	-	-	6.89±2.78	3.74±0.79	2.85±0.31	2.80±0.57	-
7.0- 3.0	-	-	2.74±0.27	3.66±0.52	3.53±0.33	3.23±0.31	3.21±0.48	-	-
3.0- 1.7	-	3.57±0.22	4.71±0.45	4.63±0.48	4.11±0.39	4.83±0.99	-	-	-
1.7- 1.0	5.30±0.20	5.18±0.27	5.39±0.35	4.45±0.26	4.89±0.36	-	-	-	-

Table 13: First fit slope for h^-

	.003-.008	.008-.013	.013-.02	.02-.032	.032-.055	.055-.1	.10-.21	.21-.4	.4-.7
$z \in$ 0.2-0.3									
81.0-16.0	-	-	-	-	-	-	4.09±0.16	4.50±0.13	-
16.0- 7.0	-	-	-	-	4.43±0.16	4.47±0.11	4.70±0.07	-	-
7.0- 3.0	-	-	4.50±0.14	4.82±0.10	4.84±0.08	5.14±0.08	-	-	-
3.0- 1.7	4.78±0.23	4.89±0.09	4.75±0.08	5.31±0.10	5.57±0.12	-	-	-	-
1.7- 1.0	4.95±0.07	5.06±0.08	5.34±0.10	6.09±0.16	-	-	-	-	-
$z \in$ 0.3-0.4									
81.0-16.0	-	-	-	-	-	-	3.09±0.20	3.62±0.18	-
16.0- 7.0	-	-	-	-	3.49±0.24	3.37±0.09	3.72±0.09	4.01±0.11	-
7.0- 3.0	-	-	3.78±0.15	3.65±0.08	3.77±0.07	3.75±0.05	3.94±0.05	-	-
3.0- 1.7	4.83±0.73	4.03±0.09	3.95±0.08	4.12±0.08	4.23±0.07	4.41±0.11	-	-	-
1.7- 1.0	4.21±0.08	4.14±0.07	4.67±0.11	4.70±0.10	5.12±0.17	-	-	-	-
$z \in$ 0.4-0.6									
81.0-16.0	-	-	-	-	-	-	3.17±0.47	2.61±0.10	-
16.0- 7.0	-	-	-	-	2.71±0.26	3.41±0.23	2.97±0.09	3.38±0.12	-
7.0- 3.0	-	-	3.25±0.16	3.22±0.13	3.10±0.11	3.34±0.10	3.84±0.24	-	-
3.0- 1.7	4.50±0.55	3.86±0.13	3.72±0.12	3.66±0.12	3.49±0.09	3.49±0.07	-	-	-
1.7- 1.0	4.45±0.11	4.02±0.09	4.11±0.09	4.03±0.08	4.03±0.11	-	-	-	-
$z \in$ 0.6-0.8									
81.0-16.0	-	-	-	-	-	-	-	-	-
16.0- 7.0	-	-	-	-	3.09±4.13	2.71±0.46	3.70±0.54	3.78±1.61	-
7.0- 3.0	-	-	3.16±0.60	5.44±0.92	3.91±0.37	3.97±0.32	3.99±0.37	-	-
3.0- 1.7	-	4.11±0.30	4.28±0.32	4.84±0.31	5.23±0.34	5.88±0.59	-	-	-
1.7- 1.0	5.75±0.21	4.97±0.20	5.55±0.26	5.36±0.25	4.91±0.33	-	-	-	-

Table 14: Second fit slope for h^+

	.003-.008	.008-.013	.013-.02	.02-.032	.032-.055	.055-.1	.10-.21	.21-.4	.4-.7
$z \in$ 0.2-0.3									
81.0-16.0	-	-	-	-	-	-	1.77±0.14	2.13±0.30	-
16.0- 7.0	-	-	-	-	1.31±0.11	1.52±0.07	1.87±0.08	-	-
7.0- 3.0	-	-	1.57±0.08	1.54±0.05	1.55±0.05	1.80±0.06	-	-	-
3.0- 1.7	1.70±0.13	1.58±0.05	1.63±0.05	1.74±0.05	2.11±0.07	-	-	-	-
1.7- 1.0	1.63±0.04	1.71±0.04	1.79±0.05	2.30±0.07	-	-	-	-	-
$z \in$ 0.3-0.4									
81.0-16.0	-	-	-	-	-	-	1.02±0.32	1.27±0.33	-
16.0- 7.0	-	-	-	-	1.24±0.16	1.00±0.11	1.45±0.11	1.73±0.31	-
7.0- 3.0	-	-	1.33±0.13	1.16±0.08	1.17±0.08	1.37±0.08	1.45±0.18	-	-
3.0- 1.7	1.57±0.19	1.36±0.08	1.18±0.08	1.44±0.07	1.65±0.09	1.57±0.22	-	-	-
1.7- 1.0	1.38±0.06	1.51±0.06	1.65±0.07	1.98±0.08	2.14±0.13	-	-	-	-
$z \in$ 0.4-0.6									
81.0-16.0	-	-	-	-	-	-	0.48±0.41	1.48±0.33	-
16.0- 7.0	-	-	-	-	0.84±0.28	1.17±0.13	1.45±0.11	1.53±0.49	-
7.0- 3.0	-	-	1.09±0.14	0.86±0.14	1.46±0.08	1.60±0.09	1.65±0.16	-	-
3.0- 1.7	1.48±0.19	1.34±0.08	1.36±0.08	1.42±0.10	1.51±0.13	1.47±0.21	-	-	-
1.7- 1.0	1.49±0.05	1.29±0.07	1.48±0.07	1.37±0.10	1.87±0.14	-	-	-	-
$z \in$ 0.6-0.8									
81.0-16.0	-	-	-	-	-	-	-	-	-
16.0- 7.0	-	-	-	-	1.52±0.08	1.43±0.10	1.44±0.17	1.71±0.75	-
7.0- 3.0	-	-	1.03±0.26	1.42±0.11	1.47±0.09	1.70±0.12	2.00±0.26	-	-
3.0- 1.7	-	1.30±0.10	1.66±0.07	1.77±0.09	1.89±0.13	2.36±0.14	-	-	-
1.7- 1.0	1.54±0.05	1.70±0.06	2.00±0.07	2.03±0.10	2.25±0.10	-	-	-	-

Table 15: Second fit slope for h^-

	.003-.008	.008-.013	.013-.02	.02-.032	.032-.055	.055-.1	.10-.21	.21-.4	.4-.7
$z \in$ 0.2-0.3									
81.0-16.0	-	-	-	-	-	-	1.32±0.24	1.37±0.35	-
16.0- 7.0	-	-	-	-	1.43±0.11	1.50±0.09	1.71±0.11	-	-
7.0- 3.0	-	-	1.48±0.09	1.61±0.05	1.66±0.05	1.98±0.07	-	-	-
3.0- 1.7	1.65±0.14	1.56±0.05	1.59±0.05	1.84±0.06	2.16±0.09	-	-	-	-
1.7- 1.0	1.56±0.04	1.69±0.05	1.94±0.06	2.47±0.08	-	-	-	-	-
$z \in$ 0.3-0.4									
81.0-16.0	-	-	-	-	-	-	0.87±0.48	1.29±0.48	-
16.0- 7.0	-	-	-	-	1.38±0.21	1.10±0.15	1.50±0.14	1.30±0.42	-
7.0- 3.0	-	-	1.32±0.12	1.26±0.09	1.36±0.08	1.41±0.10	1.23±0.22	-	-
3.0- 1.7	2.06±0.27	1.32±0.07	1.34±0.07	1.42±0.08	1.43±0.10	1.85±0.22	-	-	-
1.7- 1.0	1.37±0.06	1.41±0.06	1.78±0.08	1.93±0.09	2.15±0.15	-	-	-	-
$z \in$ 0.4-0.6									
81.0-16.0	-	-	-	-	-	-	1.26±0.24	-0.21±0.99	-
16.0- 7.0	-	-	-	-	0.96±0.37	1.44±0.10	1.11±0.17	1.13±0.35	-
7.0- 3.0	-	-	1.07±0.14	1.20±0.10	1.30±0.12	1.55±0.11	2.17±0.15	-	-
3.0- 1.7	1.41±0.26	1.38±0.07	1.40±0.08	1.49±0.09	1.50±0.12	1.11±0.23	-	-	-
1.7- 1.0	1.52±0.05	1.38±0.06	1.57±0.07	1.66±0.09	1.87±0.14	-	-	-	-
$z \in$ 0.6-0.8									
81.0-16.0	-	-	-	-	-	-	-	-	-
16.0- 7.0	-	-	-	-	1.58±0.27	1.13±0.22	1.67±0.11	2.21±0.44	-
7.0- 3.0	-	-	1.38±0.26	1.61±0.08	1.44±0.10	1.65±0.10	1.90±0.12	-	-
3.0- 1.7	-	1.45±0.11	1.43±0.10	1.65±0.08	1.98±0.07	2.26±0.09	-	-	-
1.7- 1.0	1.61±0.05	1.60±0.07	1.89±0.06	2.06±0.08	2.16±0.15	-	-	-	-

Figure 5: Differential p_T^2-dependent multiplicities for h^+ (black) and h^- (red) in x, Q^2 for z bins [0.2,0.3] (top) and [0.3,0.4] (bottom). Only statistical errors are shown.

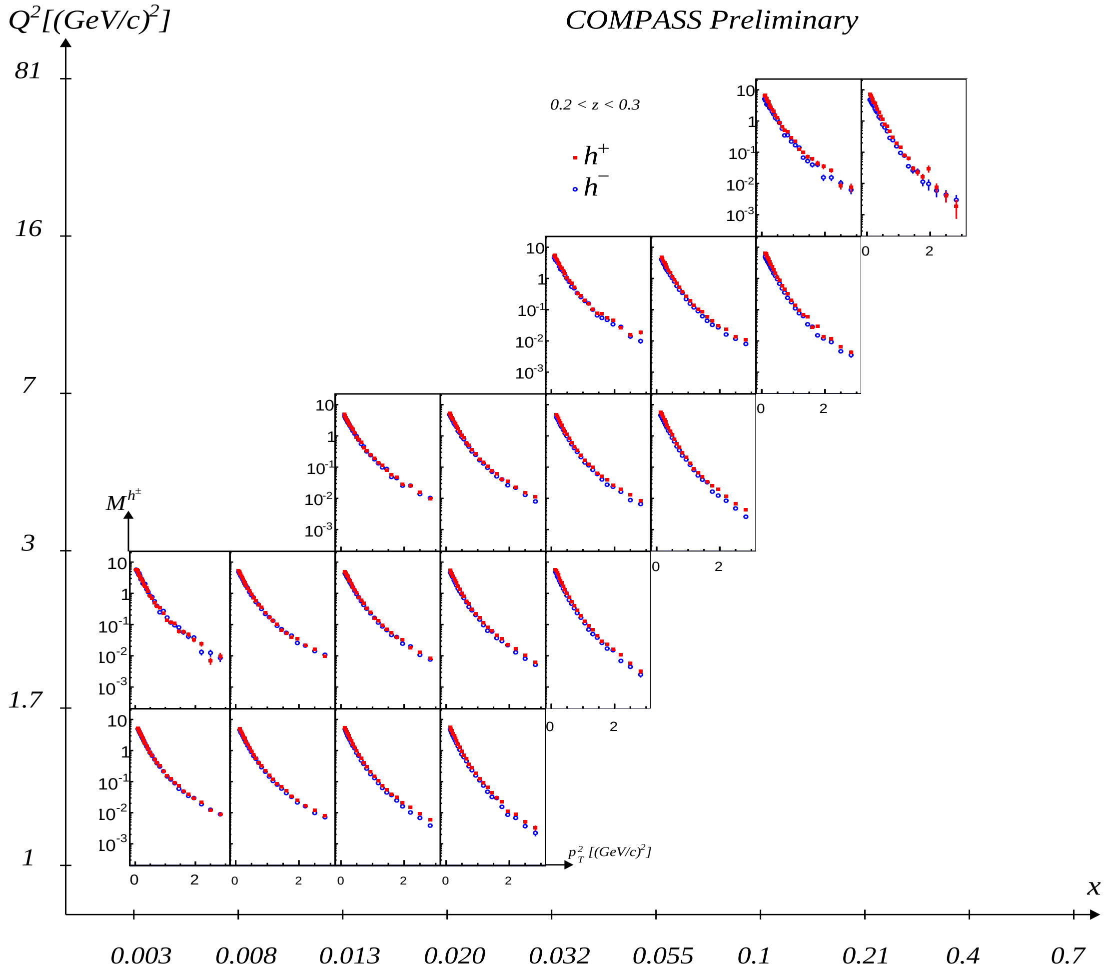

(a)

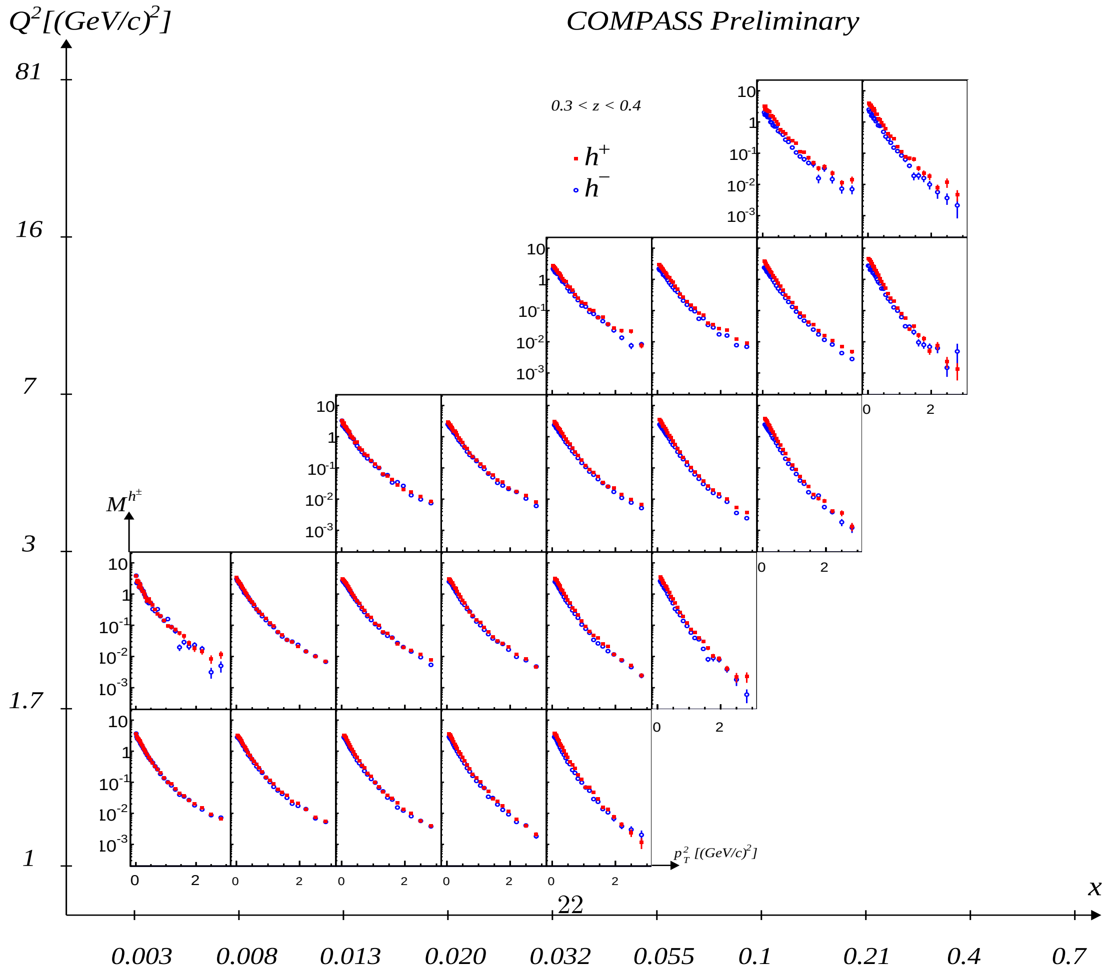

(b)

Figure 6: Differential p_T^2-dependent multiplicities for h^+ (black) and h^- (red) in x, Q^2 for z bins [0.4,0.6] (top) and [0.6,0.8] (bottom). Only statistical errors are shown.

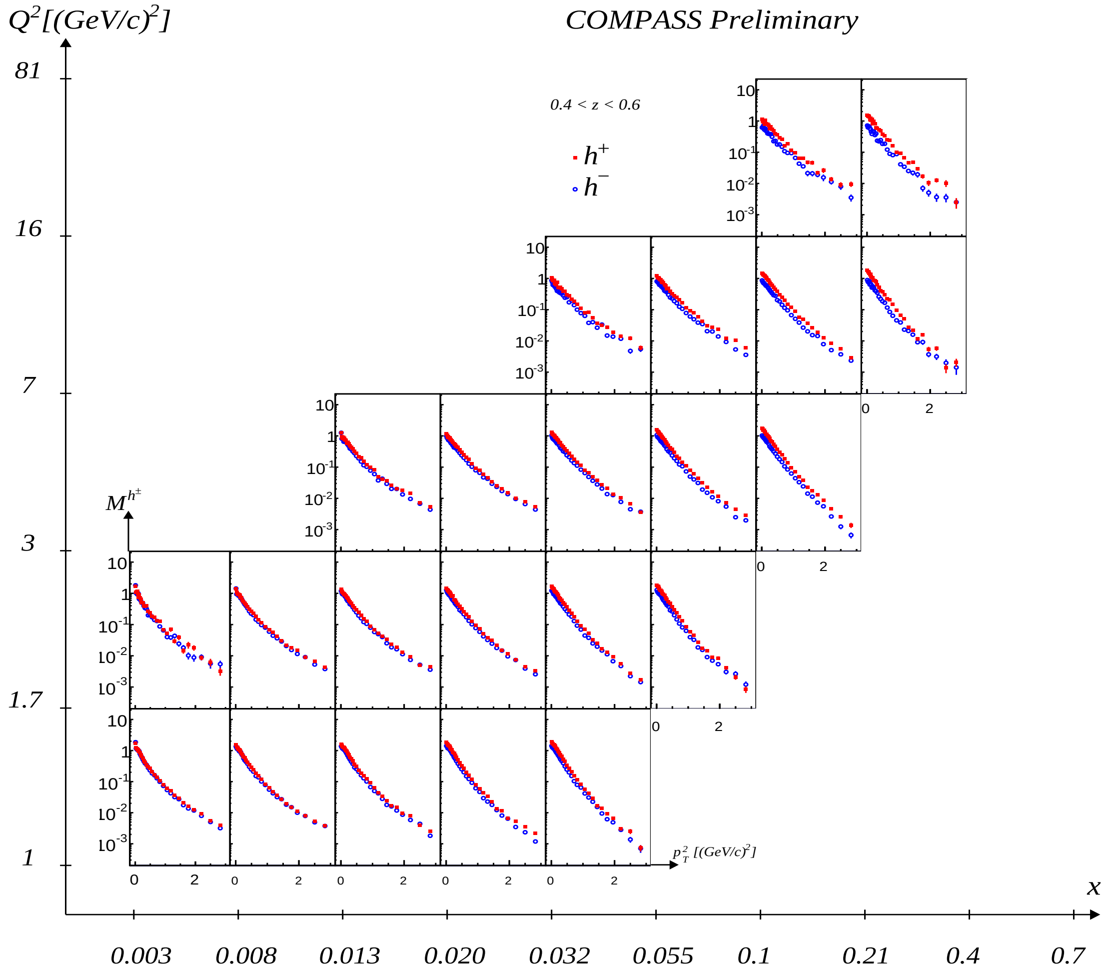

(a)

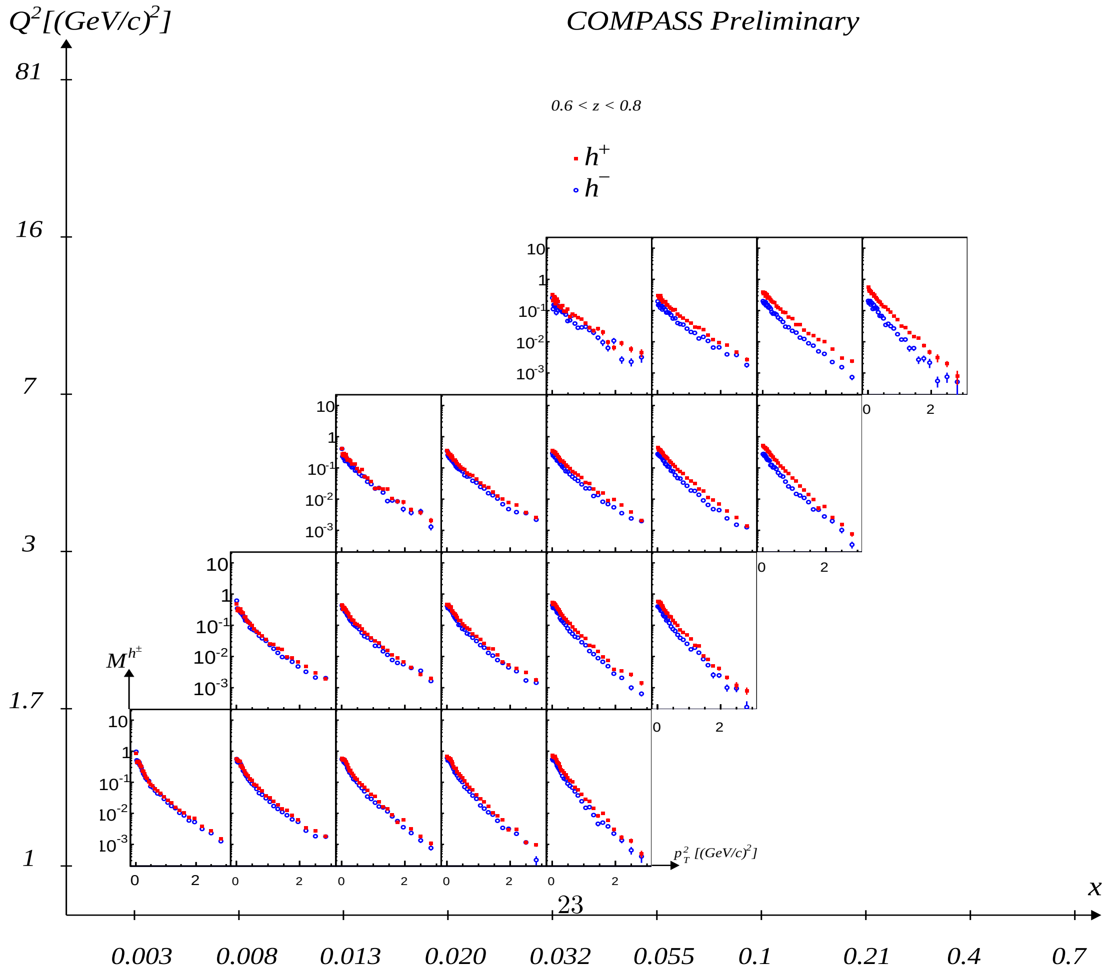

(b)

Figure 7: Differential p_T^2-dependent multiplicities for h^+ (black) and h^- (red) in x, Q^2 for z bins [0.2,0.3] (top) and [0.3,0.4] (bottom). Statistical and relative systematic uncertainties are shown.

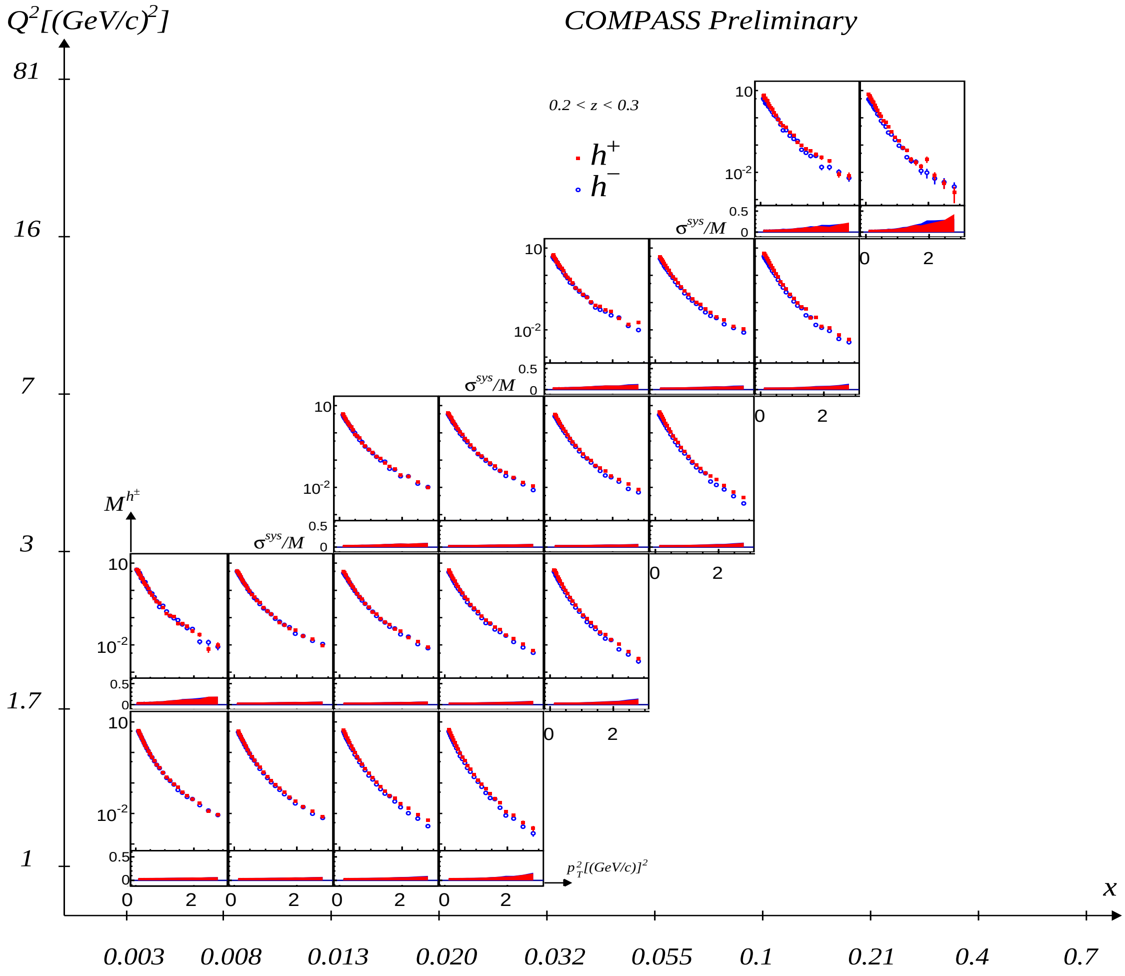

(a)

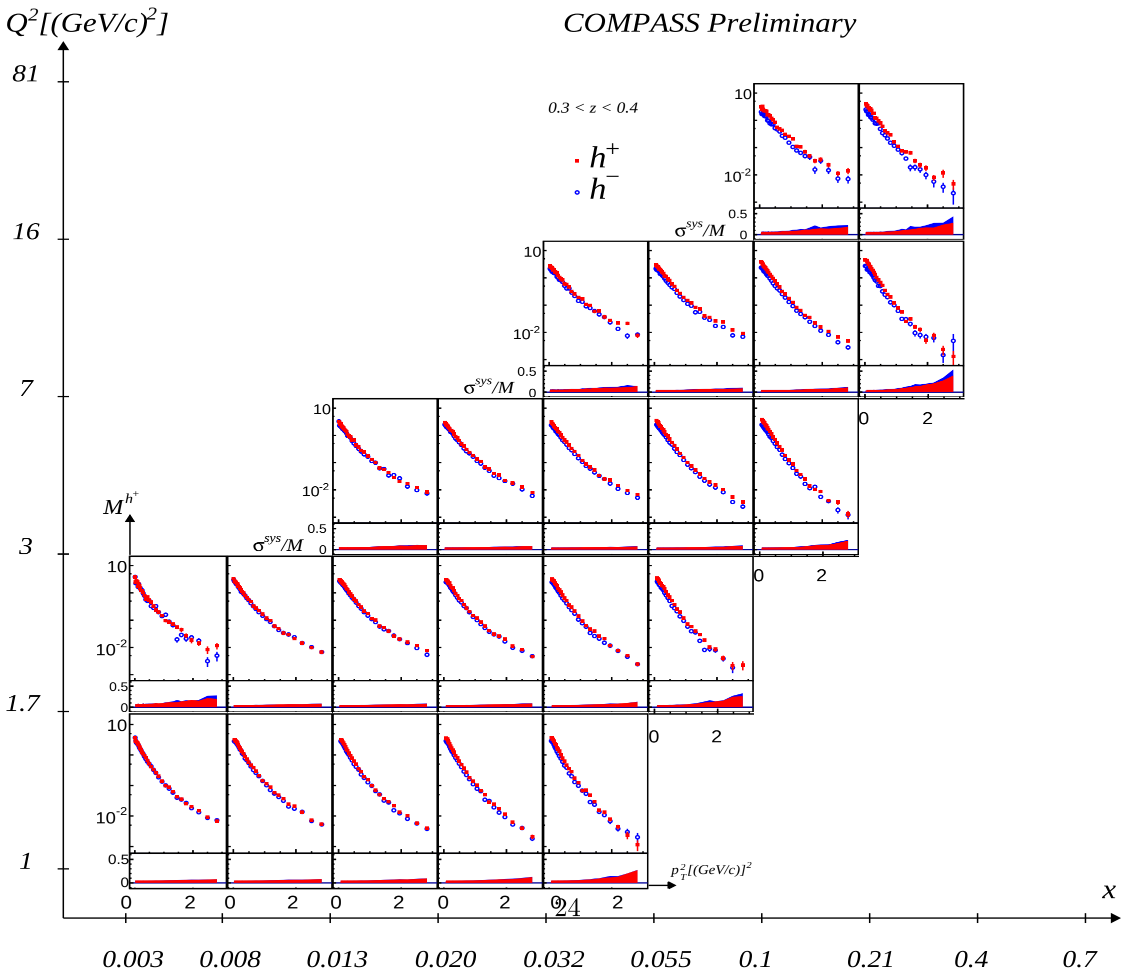

(b)

Figure 8: Differential p_T^2-dependent multiplicities for h^+ (black) and h^- (red) in x, Q^2 for z bins [0.4,0.6] (top) and [0.6,0.8] (bottom). Statistical and relative systematic uncertainties are shown.

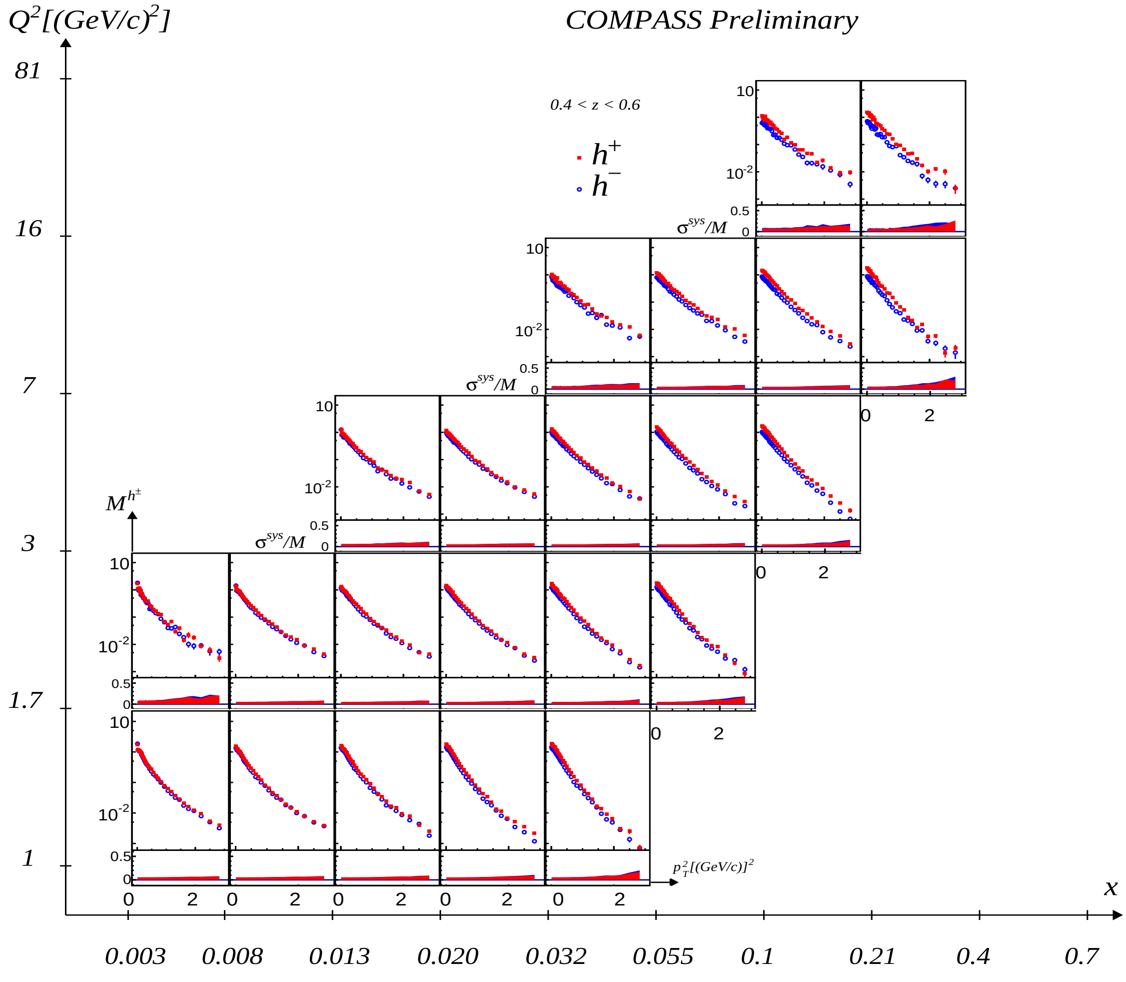

(a)

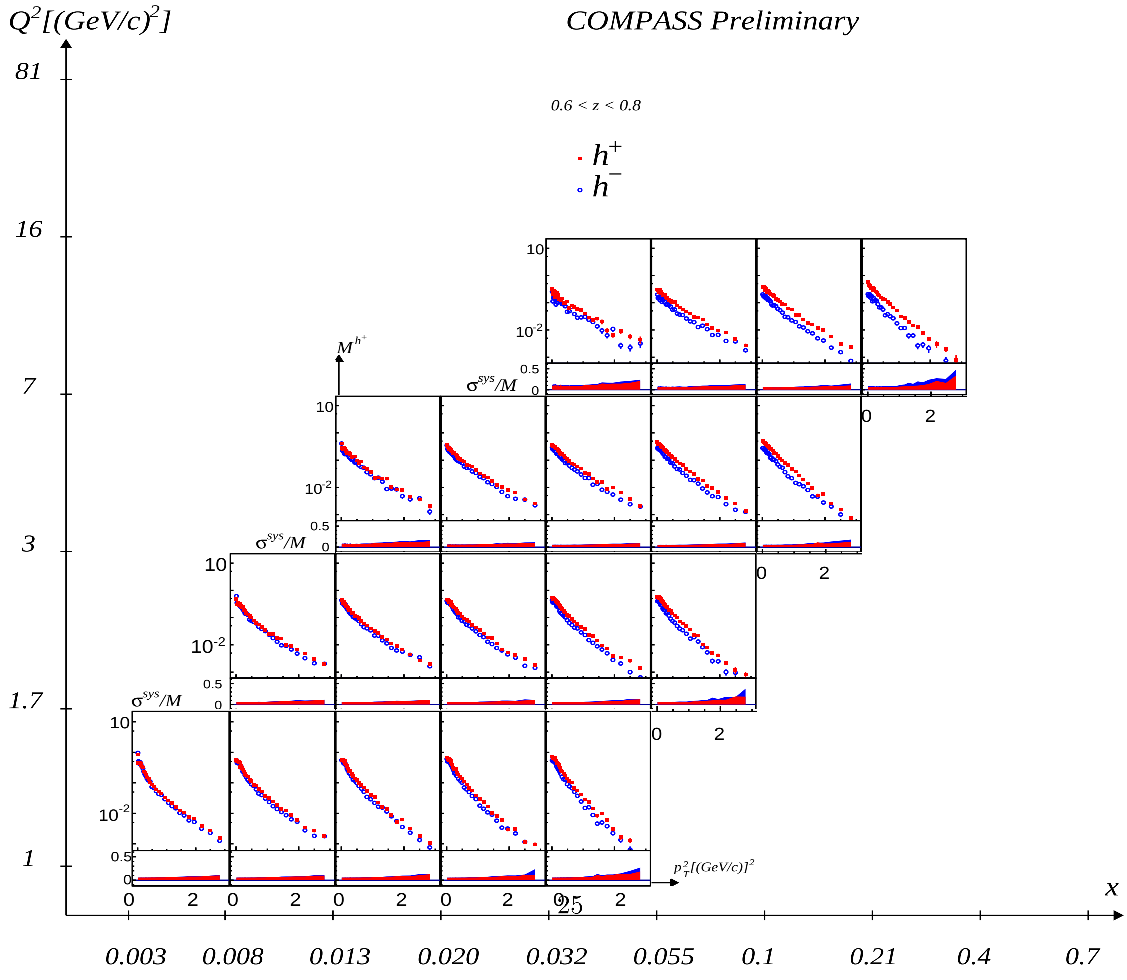

(b)

Figure 9: Differential p_T^2-dependent multiplicities for h^+ (black) and h^- (red) in x, Q^2 for z bins [0.2,0.3] (top) and [0.3,0.4] (bottom). Only statistical errors are shown.

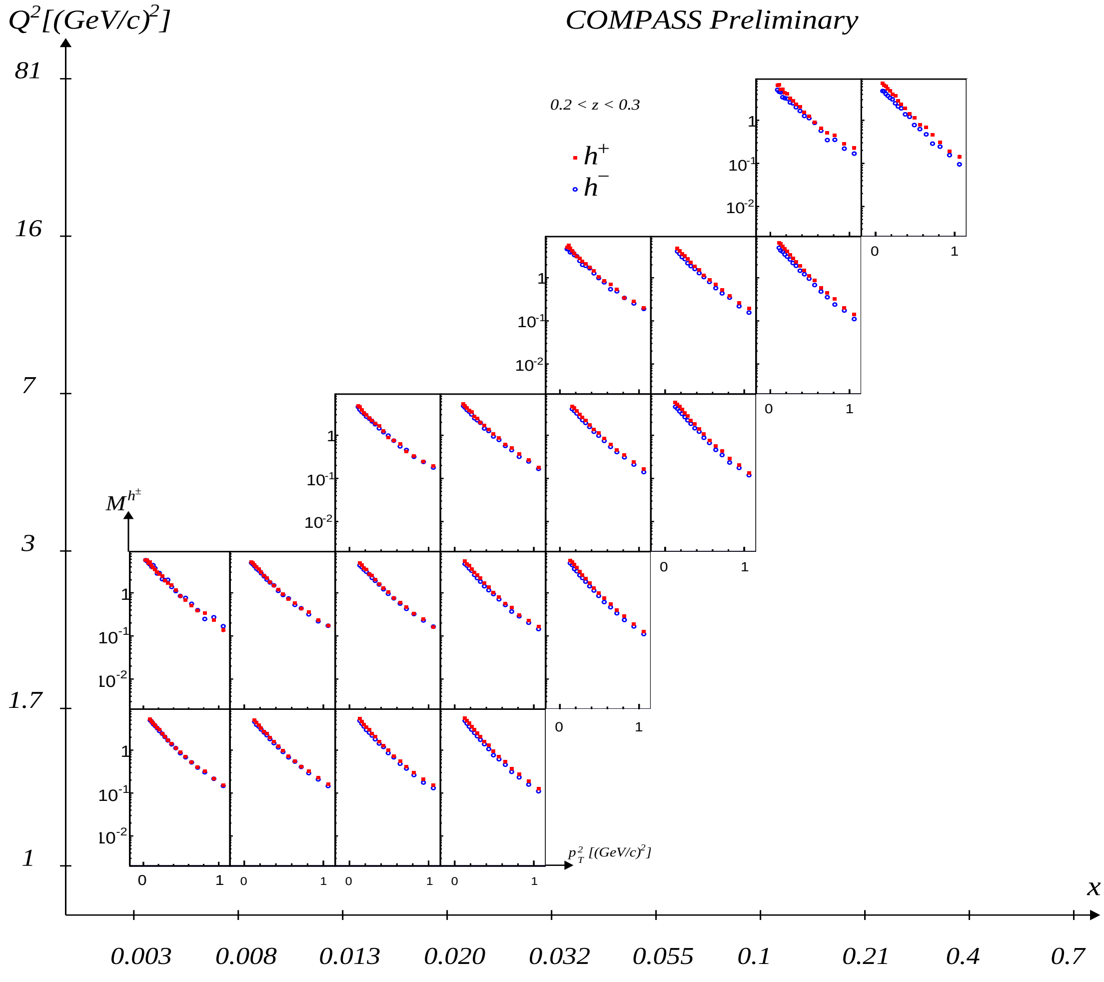

(a)

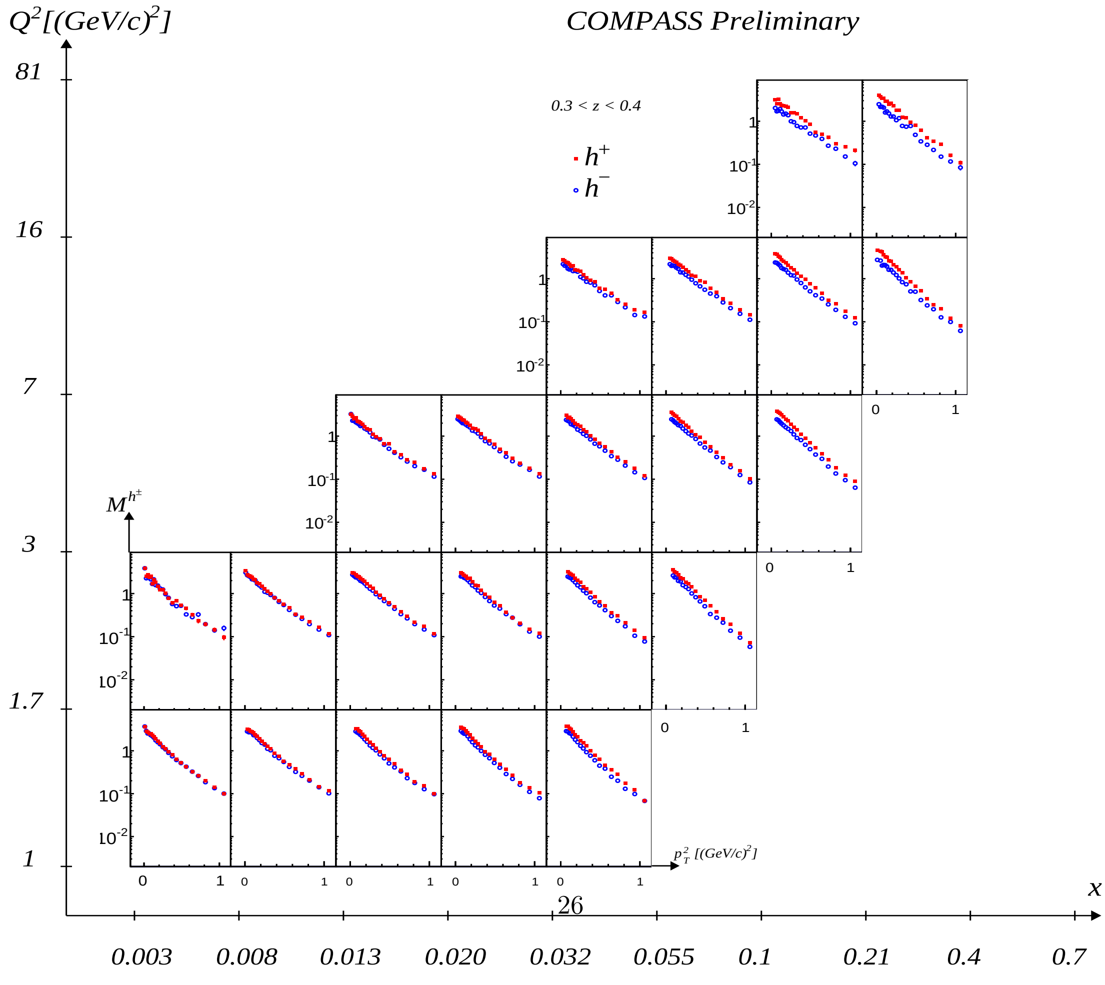

(b)

Figure 10: Differential p_T^2-dependent multiplicities for h^+ (black) and h^- (red) in x, Q^2 for z bins [0.4,0.6] (top) and [0.6,0.8] (bottom). Only statistical errors are shown.

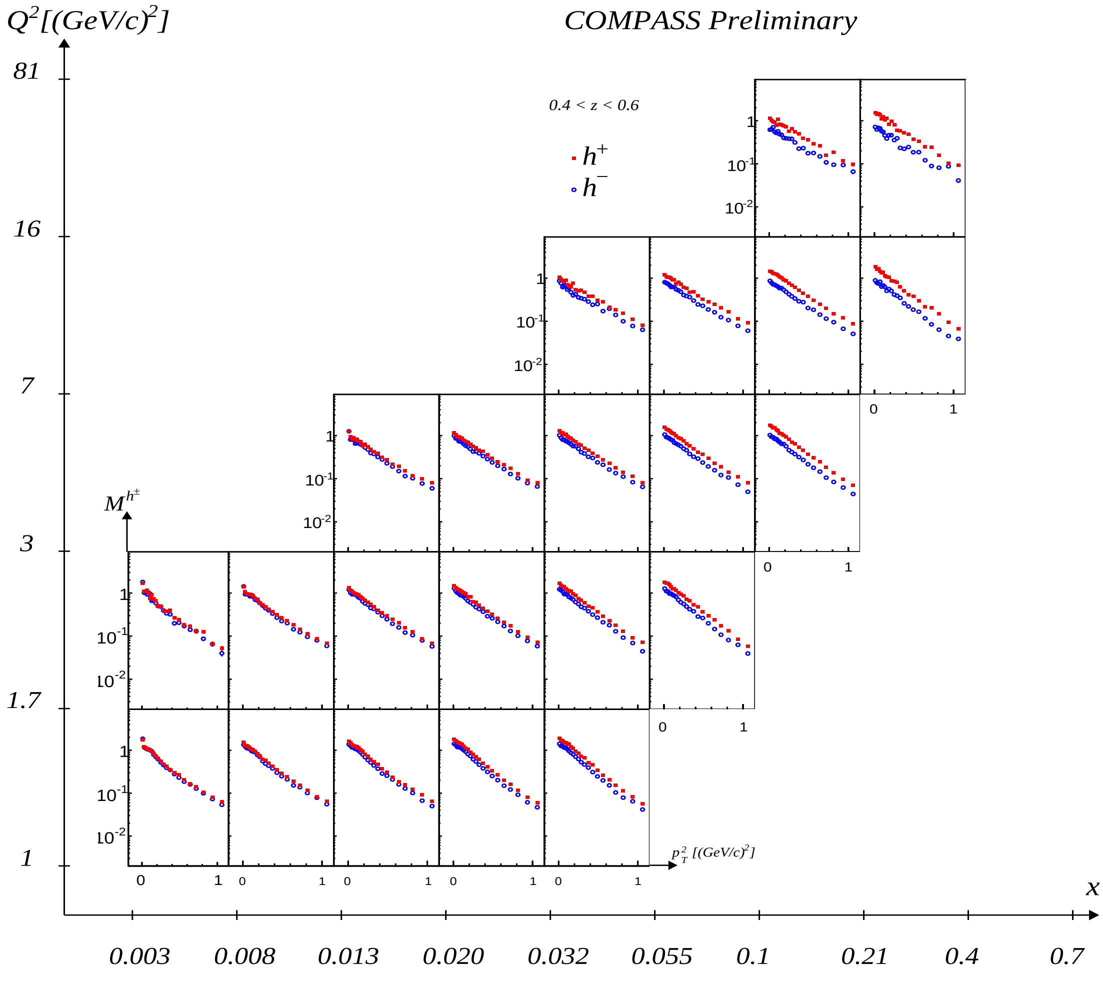

(a)

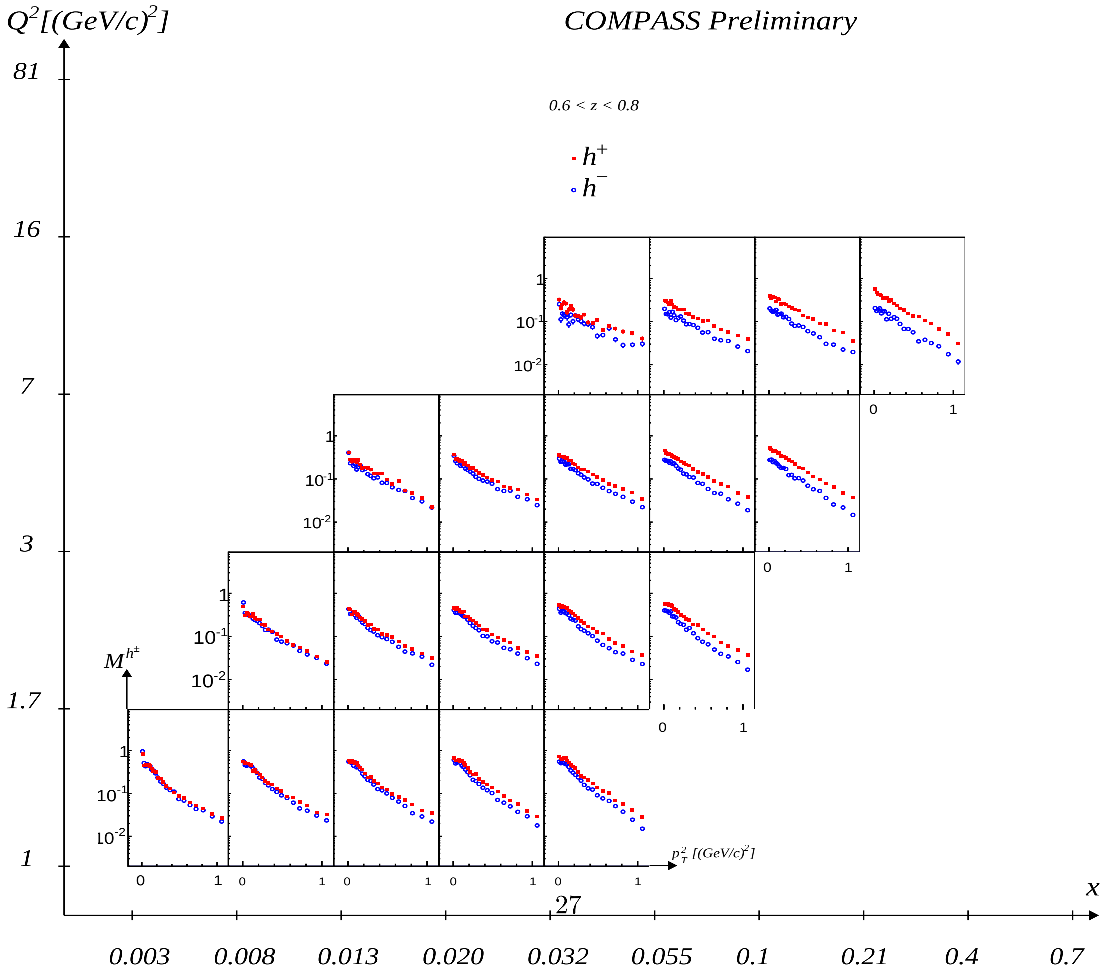

(b)

Figure 11: Differential p_T^2-dependent multiplicities for h^+ (black) and h^- (red) in x, Q^2 for z bins [0.2,0.3] (top) and [0.3,0.4] (bottom). Statistical and relative systematic errors are shown.

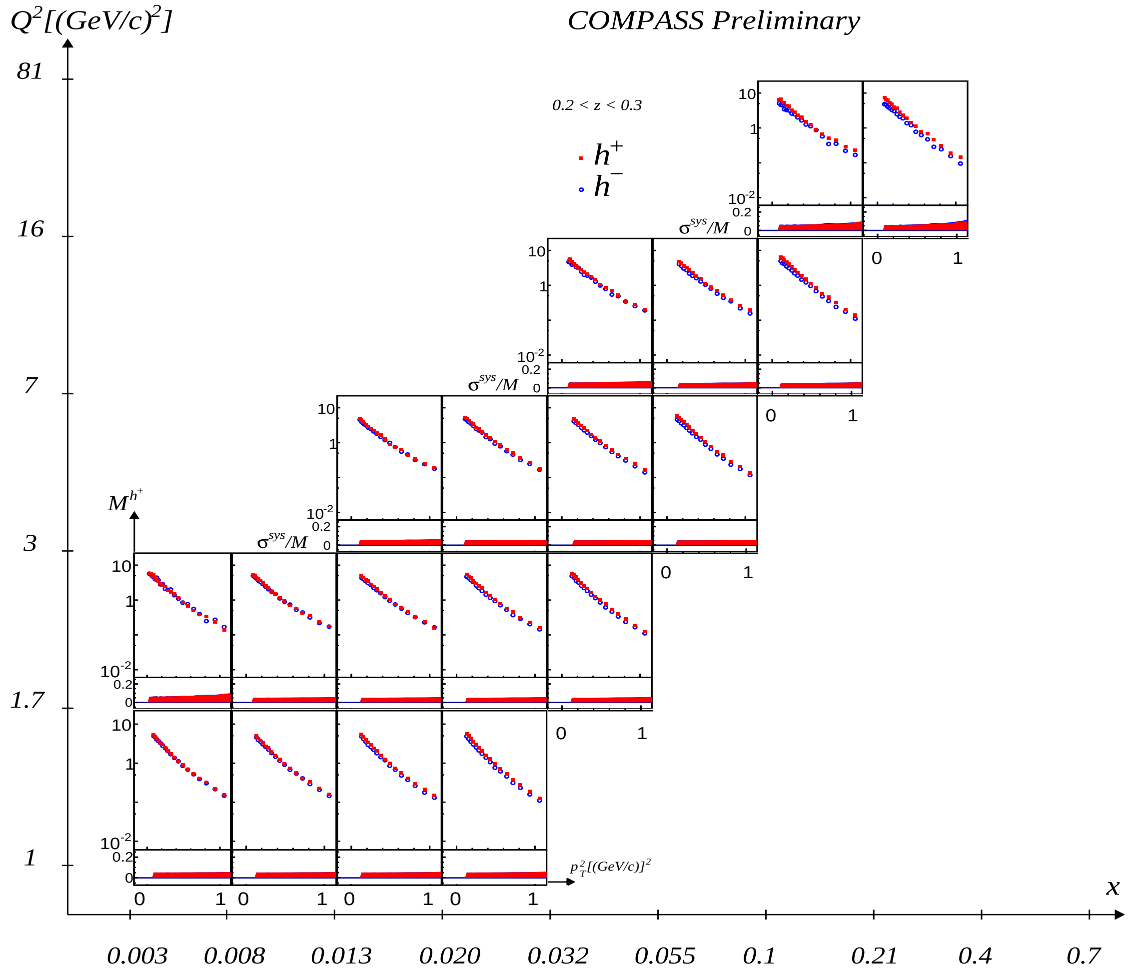

(a)

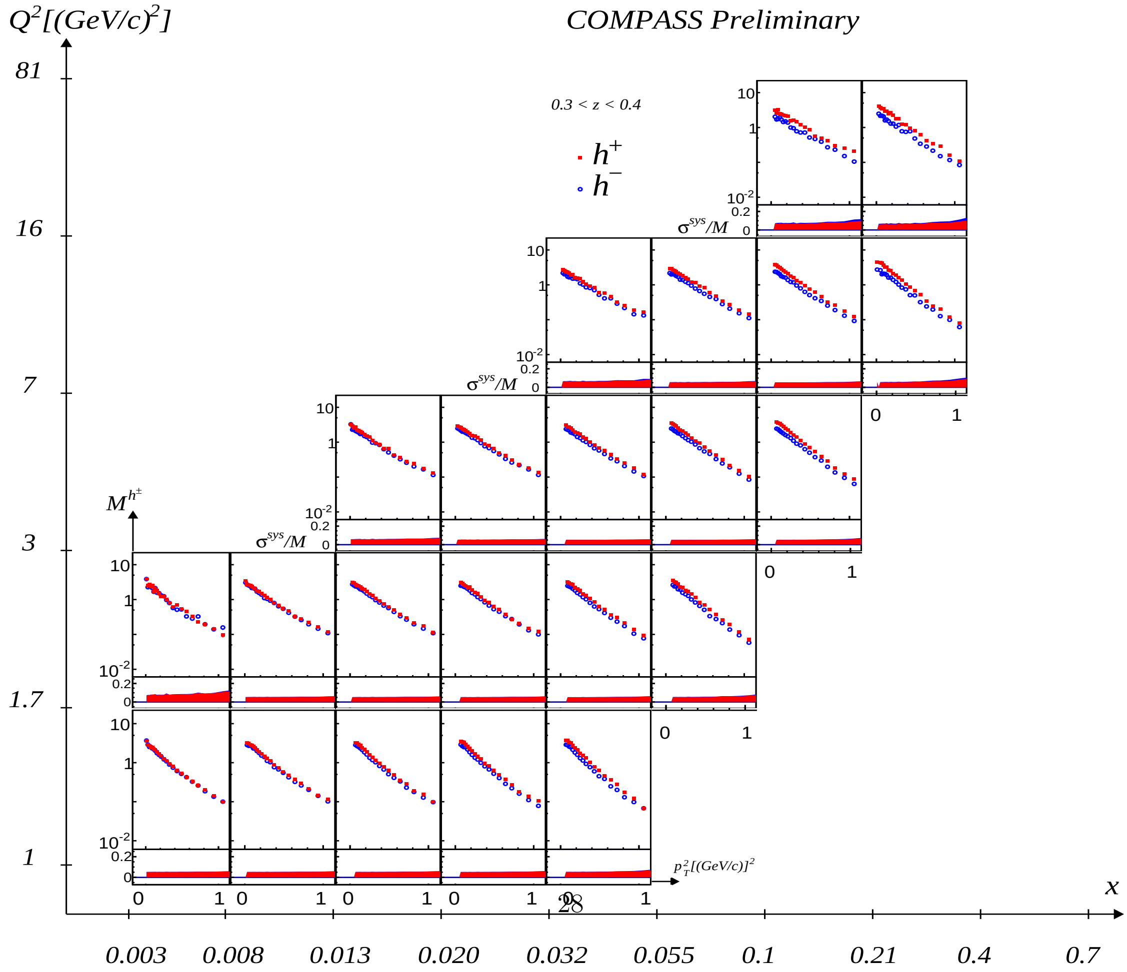

(b)

Figure 12: Differential p_T^2-dependent multiplicities for h^+ (black) and h^- (red) in x, Q^2 for z bins [0.4,0.6] (top) and [0.6,0.8] (bottom). Statistical and relative systematic errors are shown.

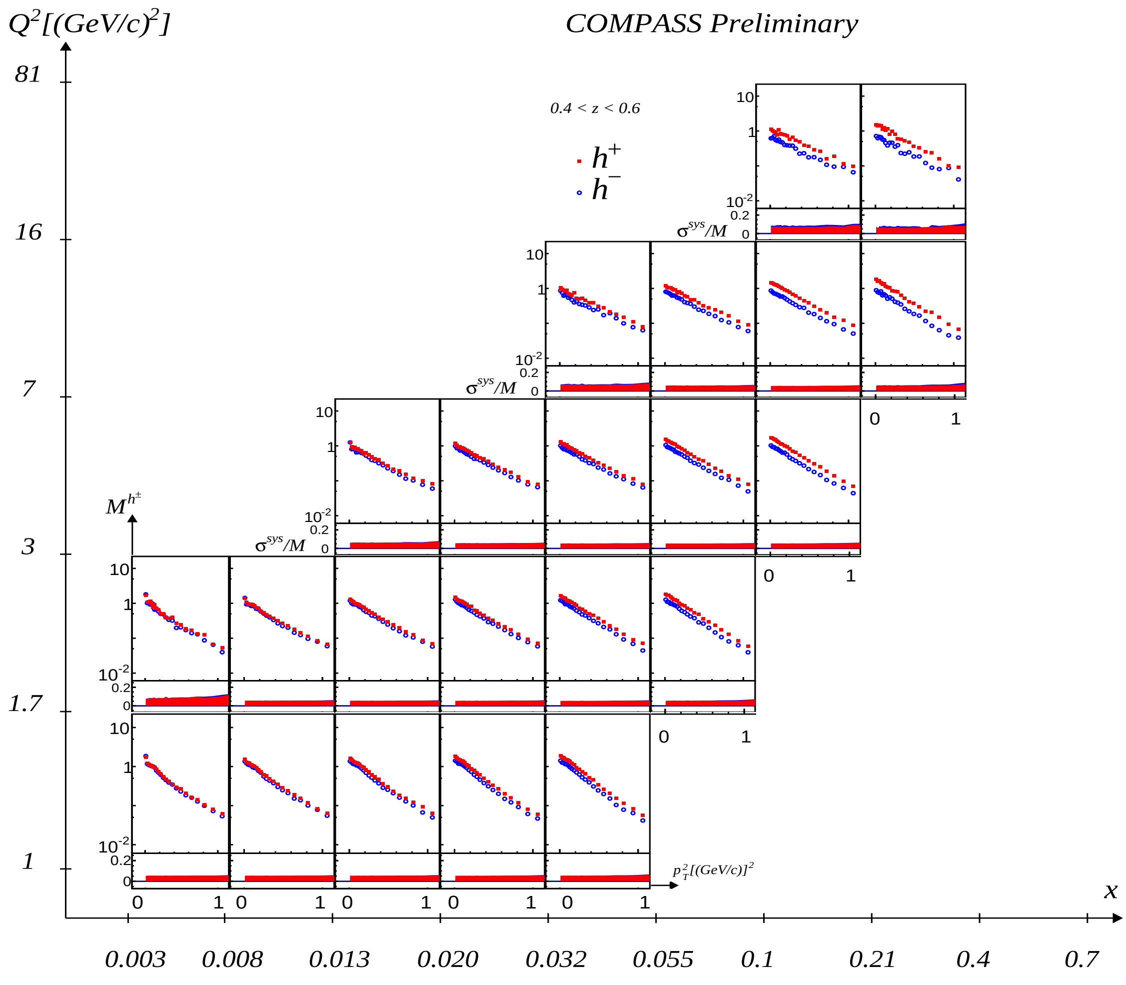

(a)

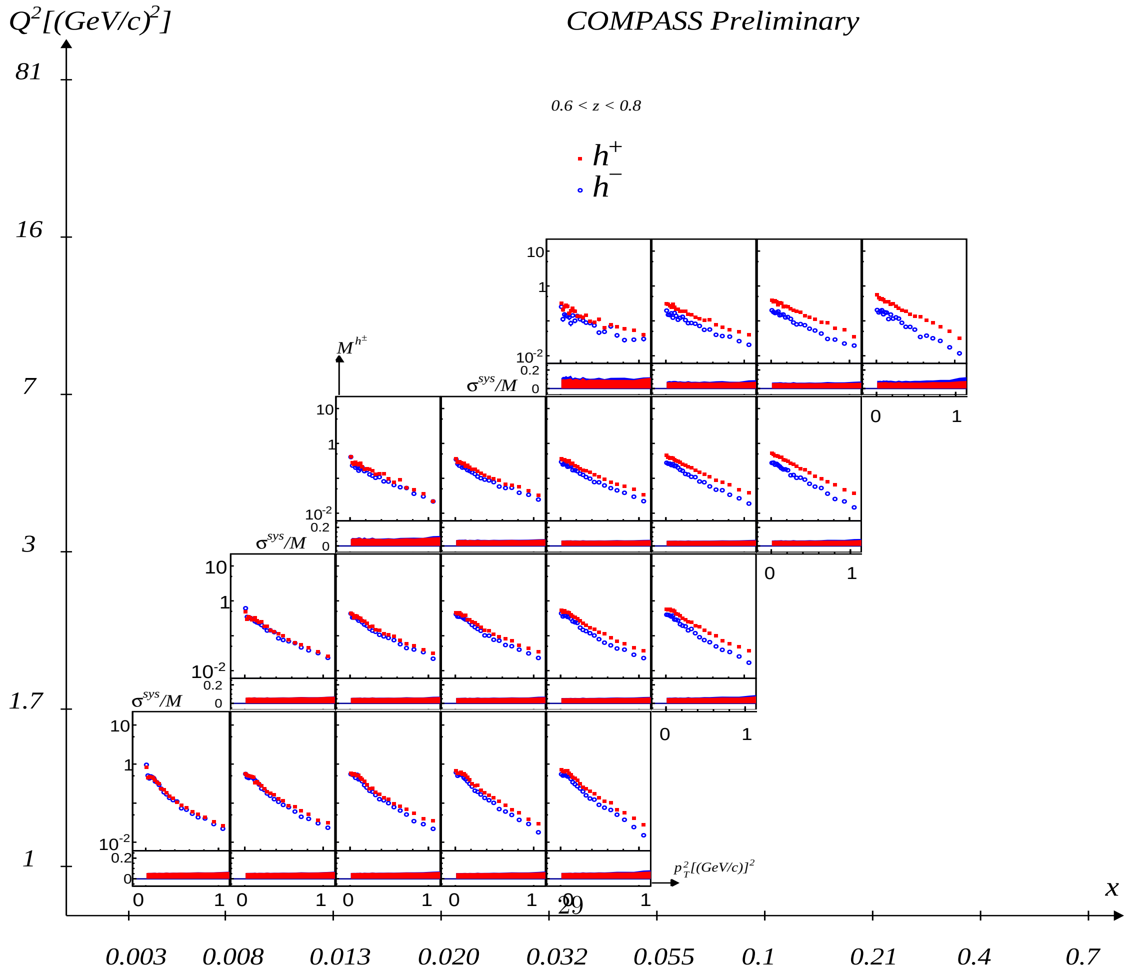

(b)

Figure 13: Ratio of positive to negative p_T^2-dependent hadron multiplicities in x, Q^2 for z bins [0.2,0.3] (top) and [0.3,0.4] (bottom). Only statistical errors are shown.

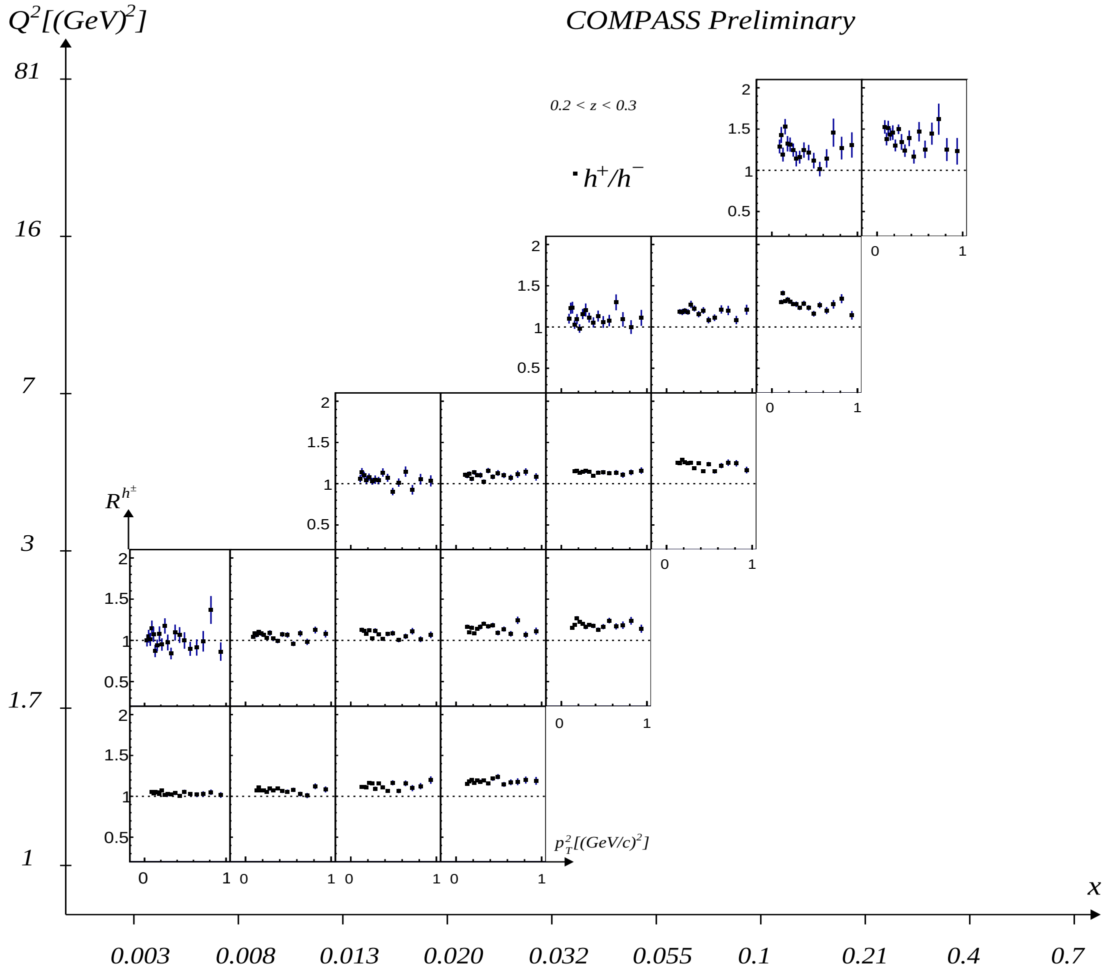

(a)

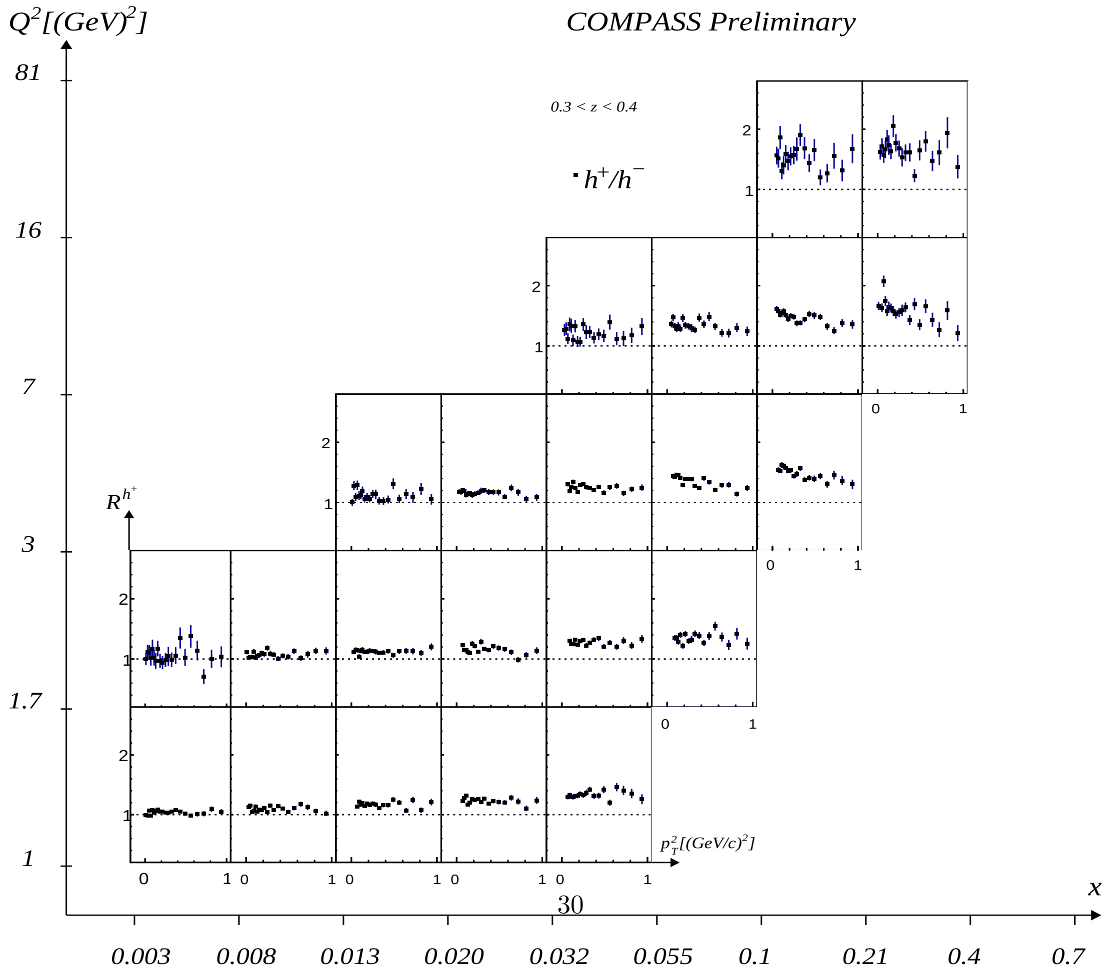

(b)

Figure 14: Ratio of positive to negative p_T^2-dependent hadron multiplicities in x, Q^2 for z bins [0.4,0.6] (top) and [0.6,0.8] (bottom). Only statistical errors are shown.

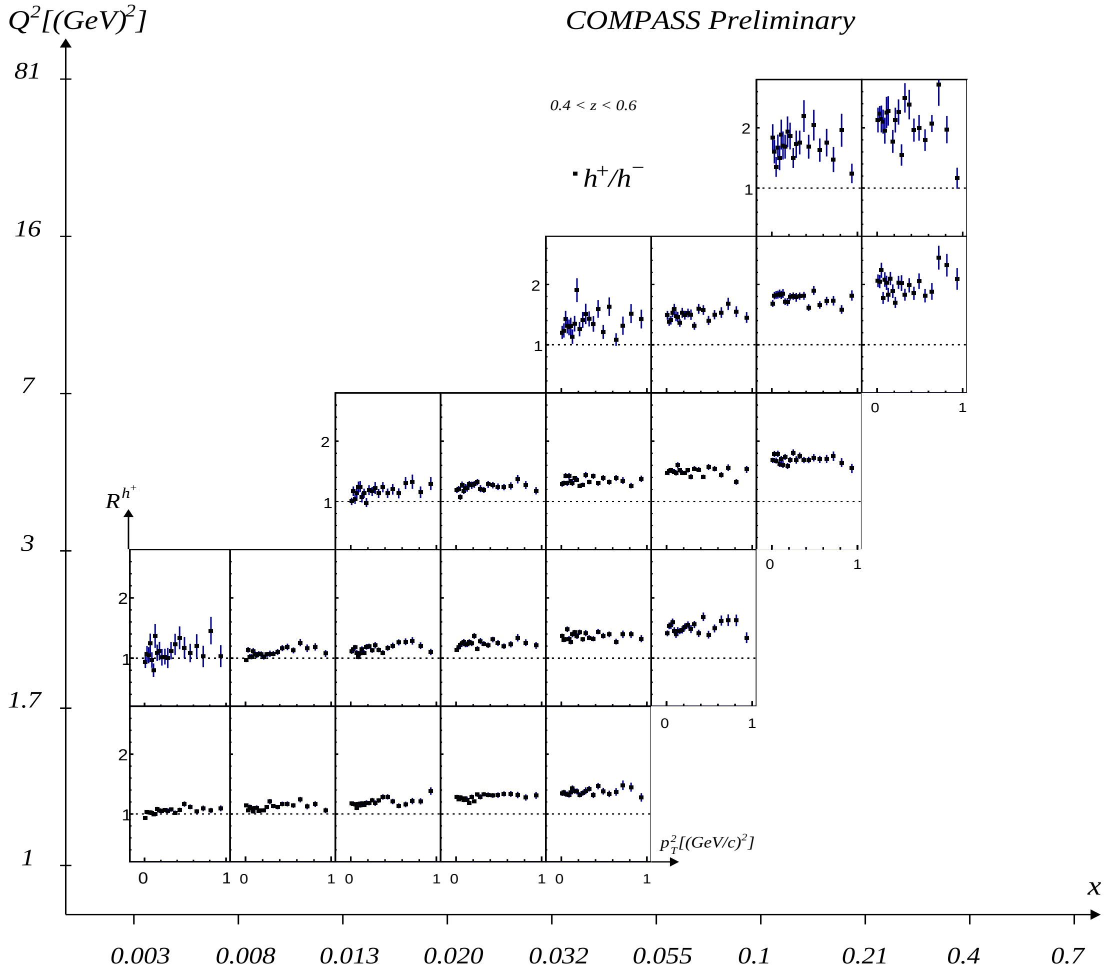

(a)

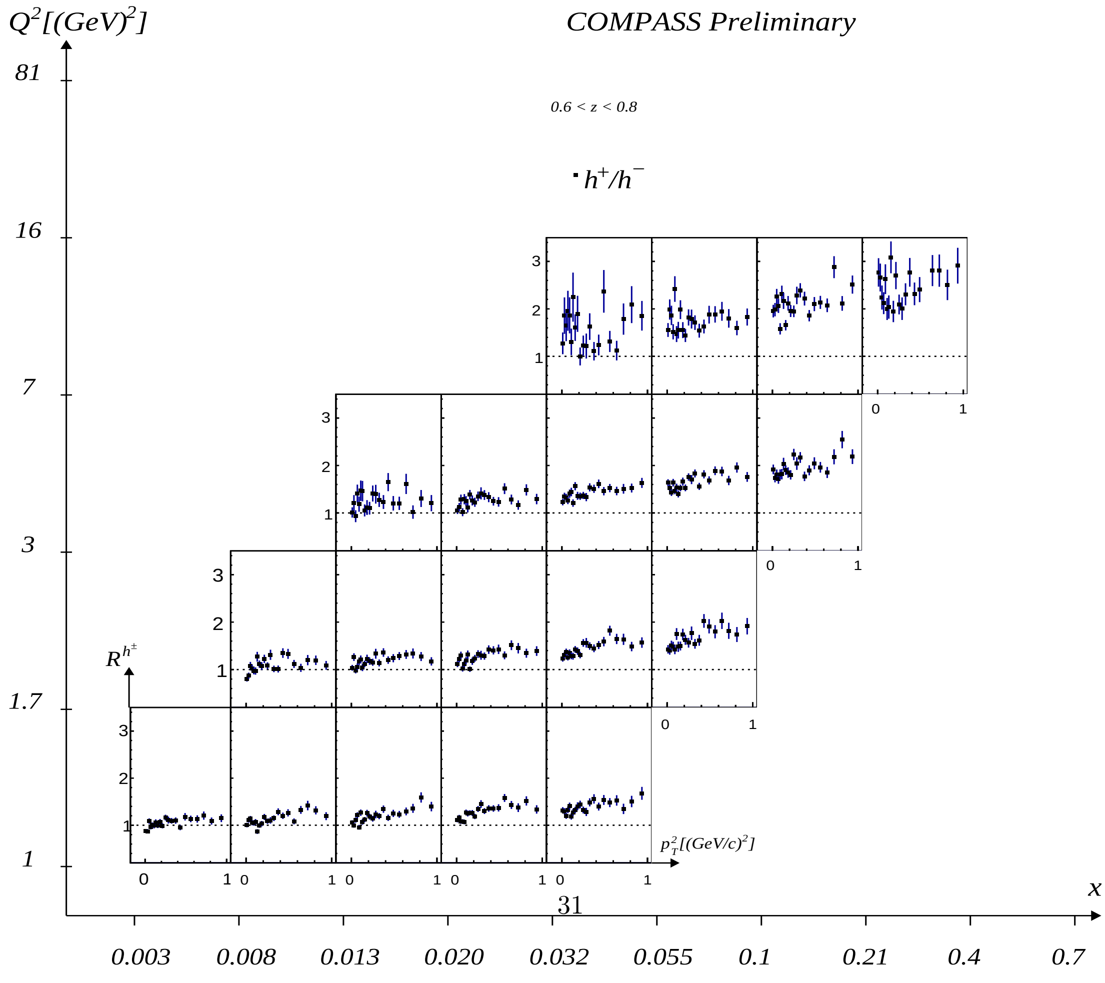

(b)

Figure 15: $M^{h^+}(p_T^2)$ in x, Q^2 and z bins. In each (Q^2, z) bin, $M^{h^+}(x)$ (small to large x) are scaled by $(10^1,\ 10^0,\ 10^{-1}, 10^{-2}, 10^{-3}, 10^{-4}, 10^{-5}, 10^{-6}, 10^{-7})$ respectively for visibility, with only statistical errors.

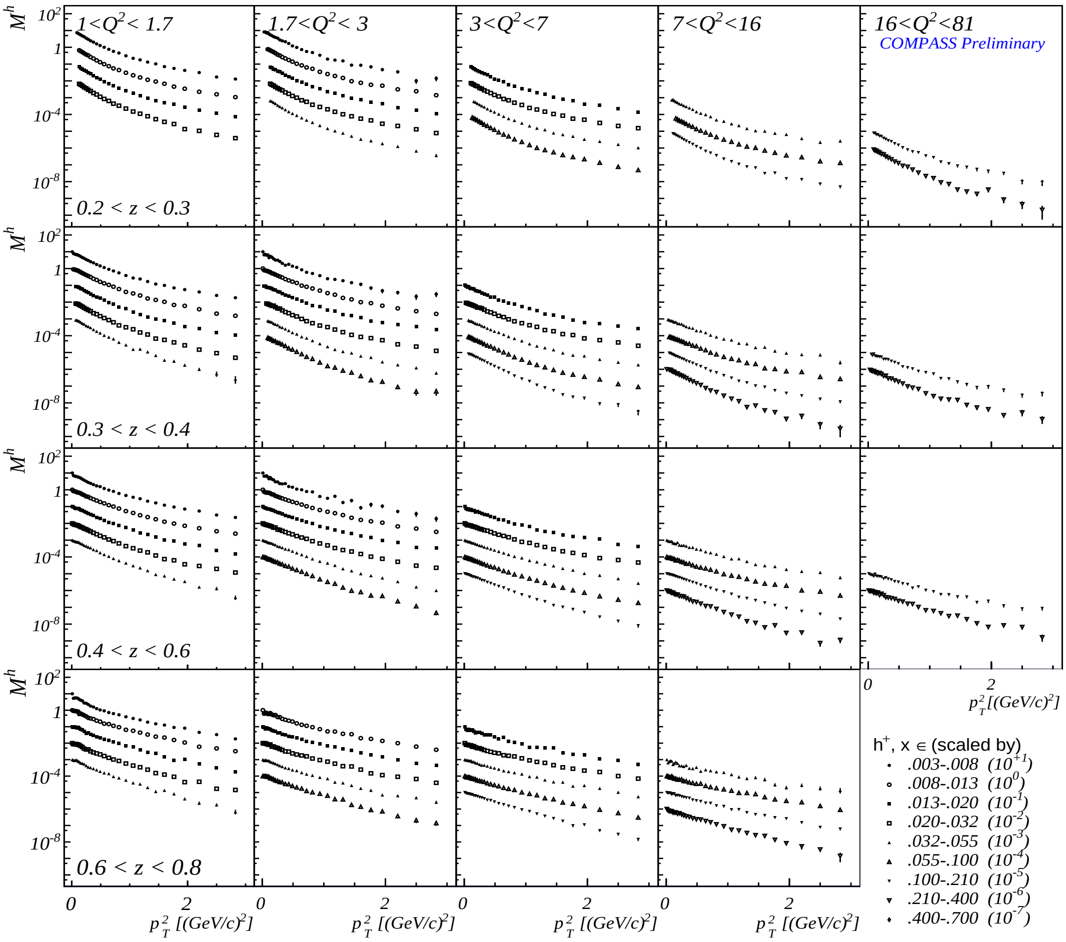

(a) positive hadrons

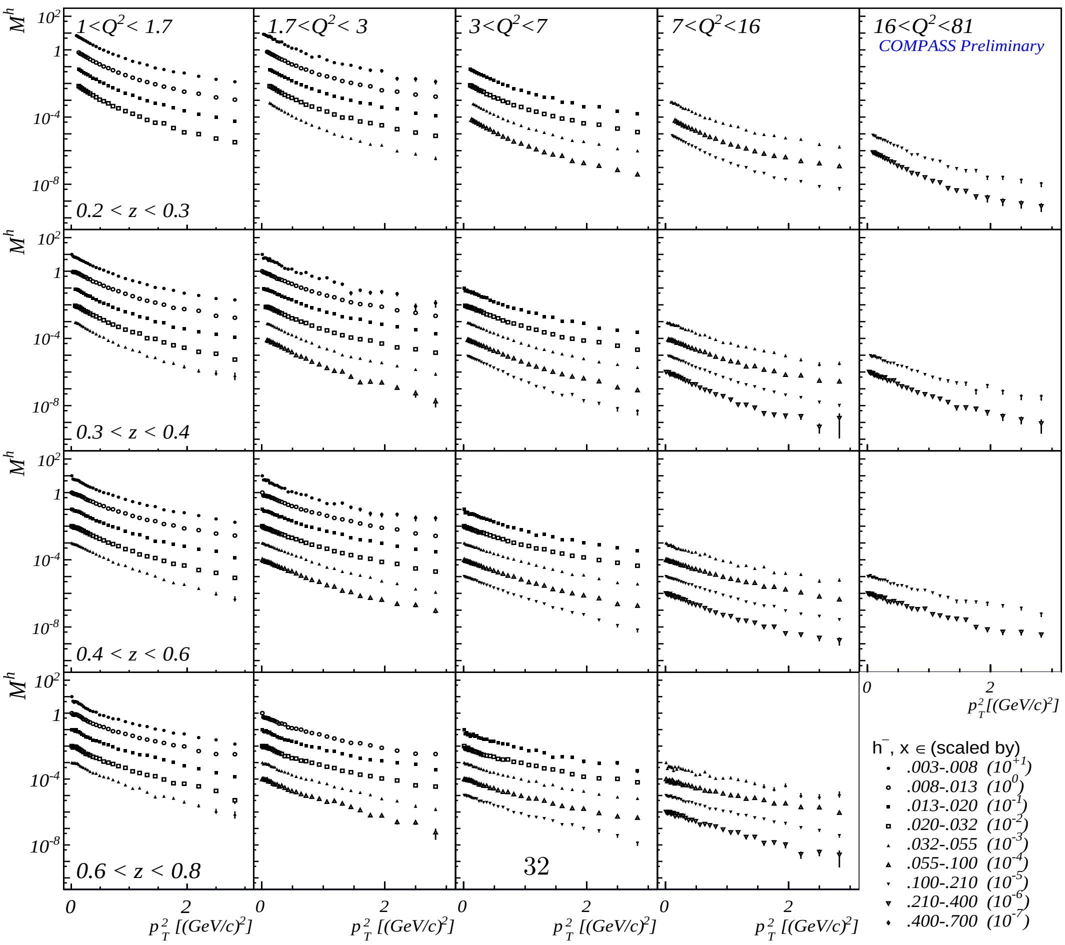

(b) negative hadrons

Figure 16: $M^{h^+}(p_T^2)$ in x, Q^2 and z bins. In each (Q^2, z) bin, $M^{h^+}(x)$ (small to large x) are scaled by (10^1, 10^0, 10^{-1},10^{-2},10^{-3},10^{-4},10^{-5},10^{-6},10^{-7}) respectively for visibility and fitted with $ae^{-\alpha p_T^2} + be^{-\beta p_T^2}$. Only statistical errors are shown and used in the fit.

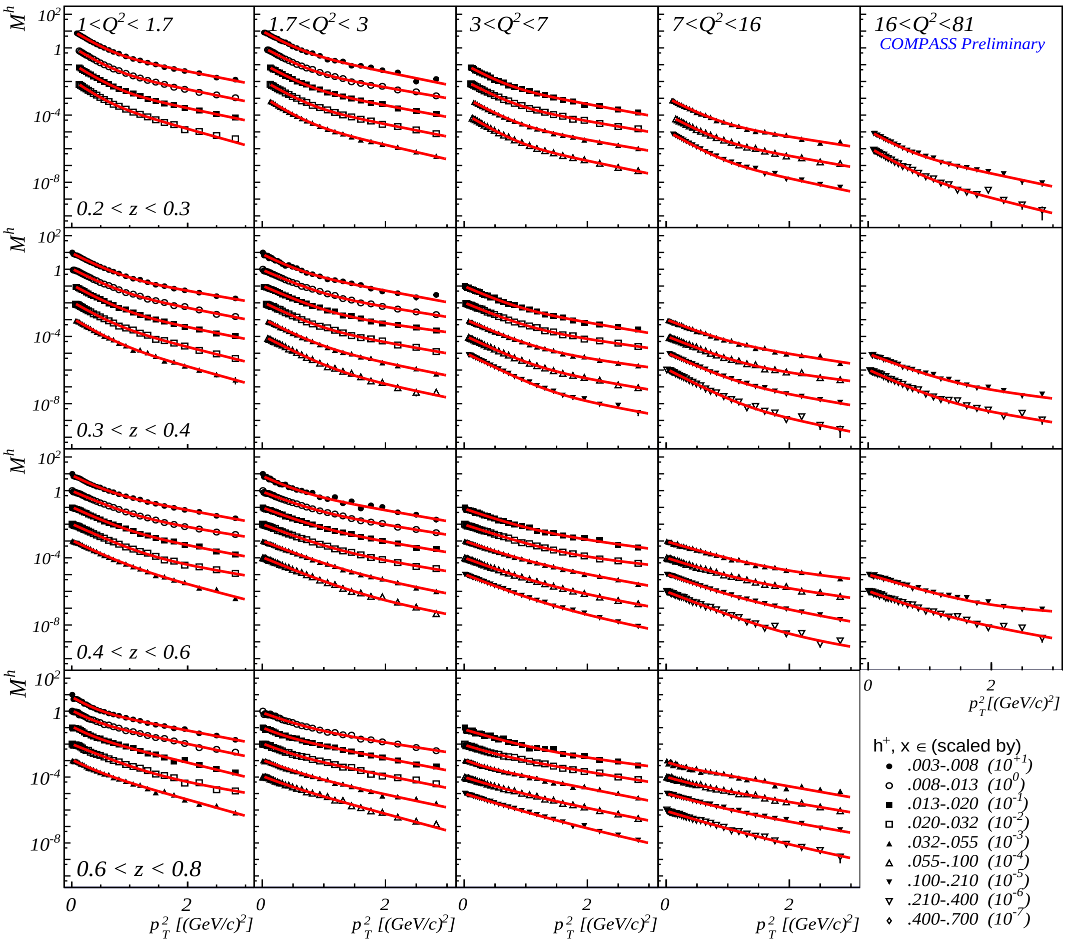

(a) positive hadrons

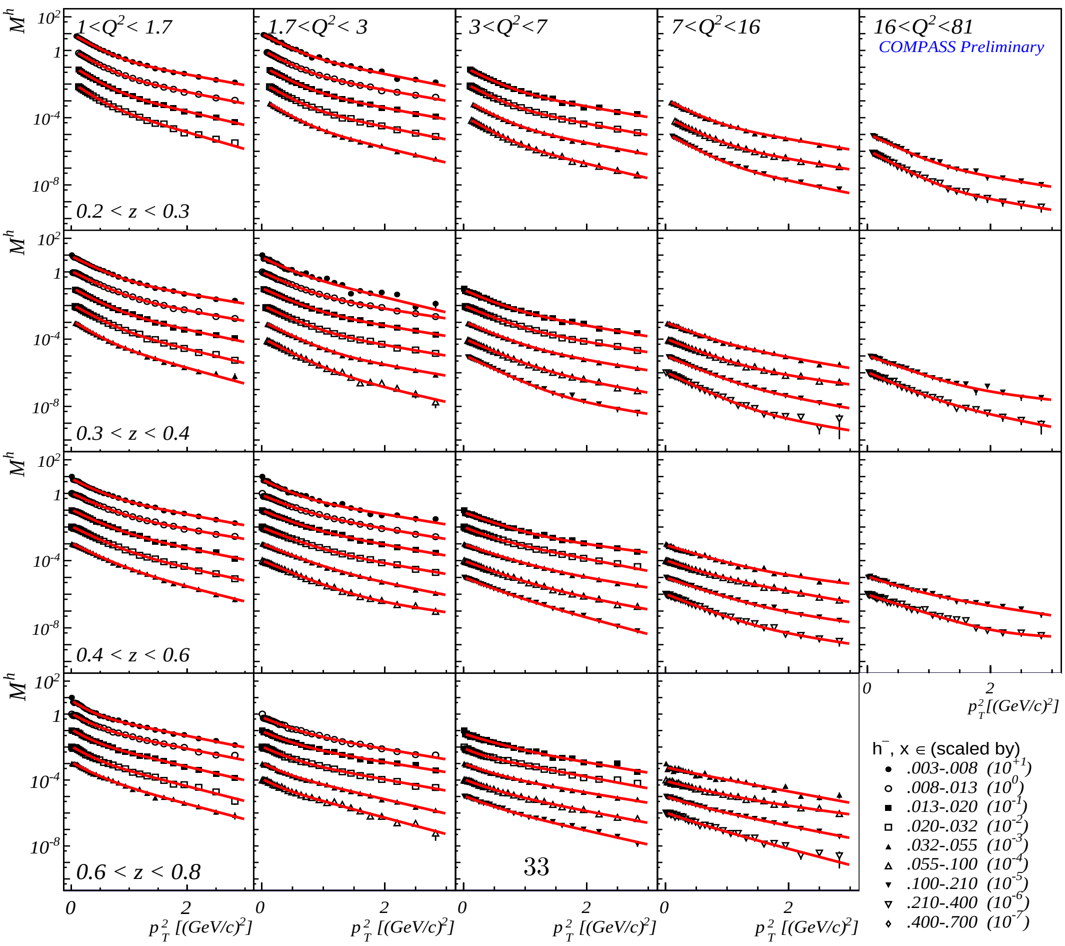

(b) negative hadrons

Figure 17: Differential p_T^2-dependent hadron multiplicities in different x, Q^2 and z bins fitted with two-exponentials function ($ae^{-\alpha p_T^2} + be^{-\beta p_T^2}$). Only statistical errors are shown and used in the fits.

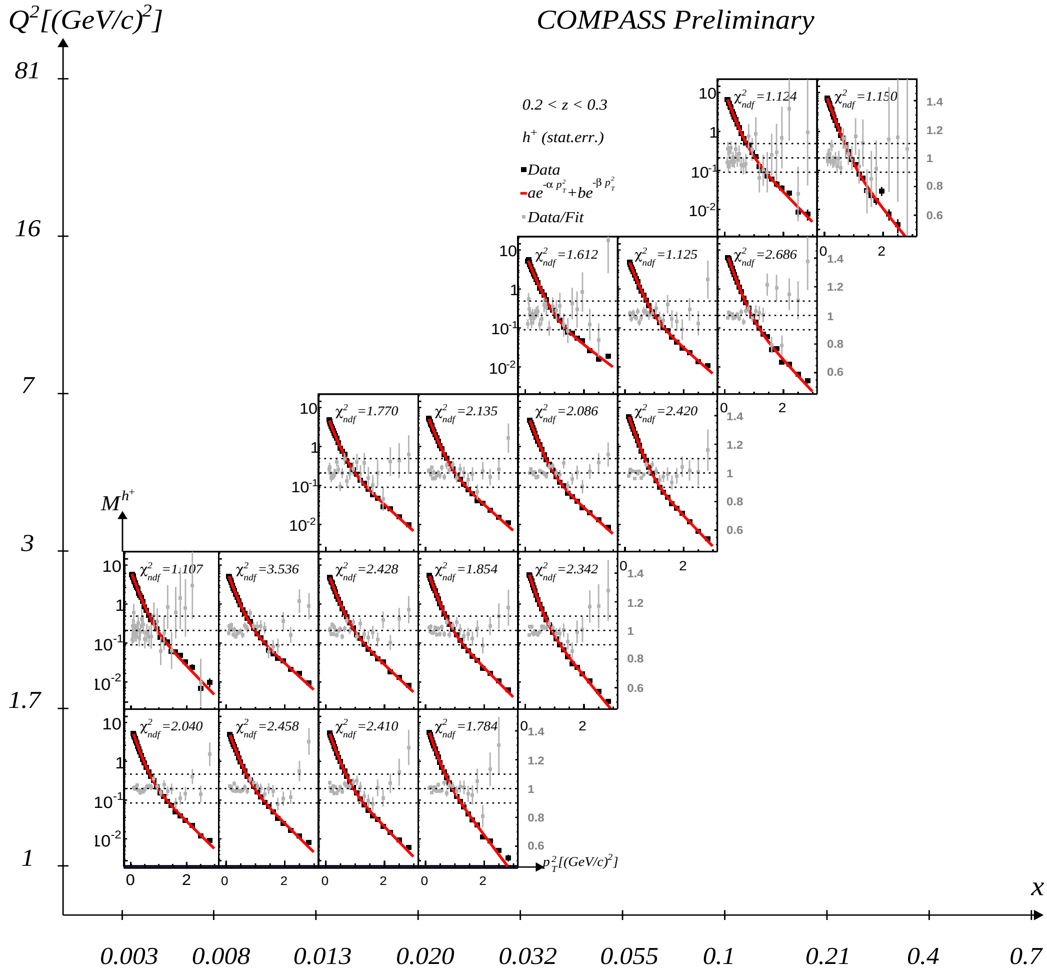

(a) positive hadrons

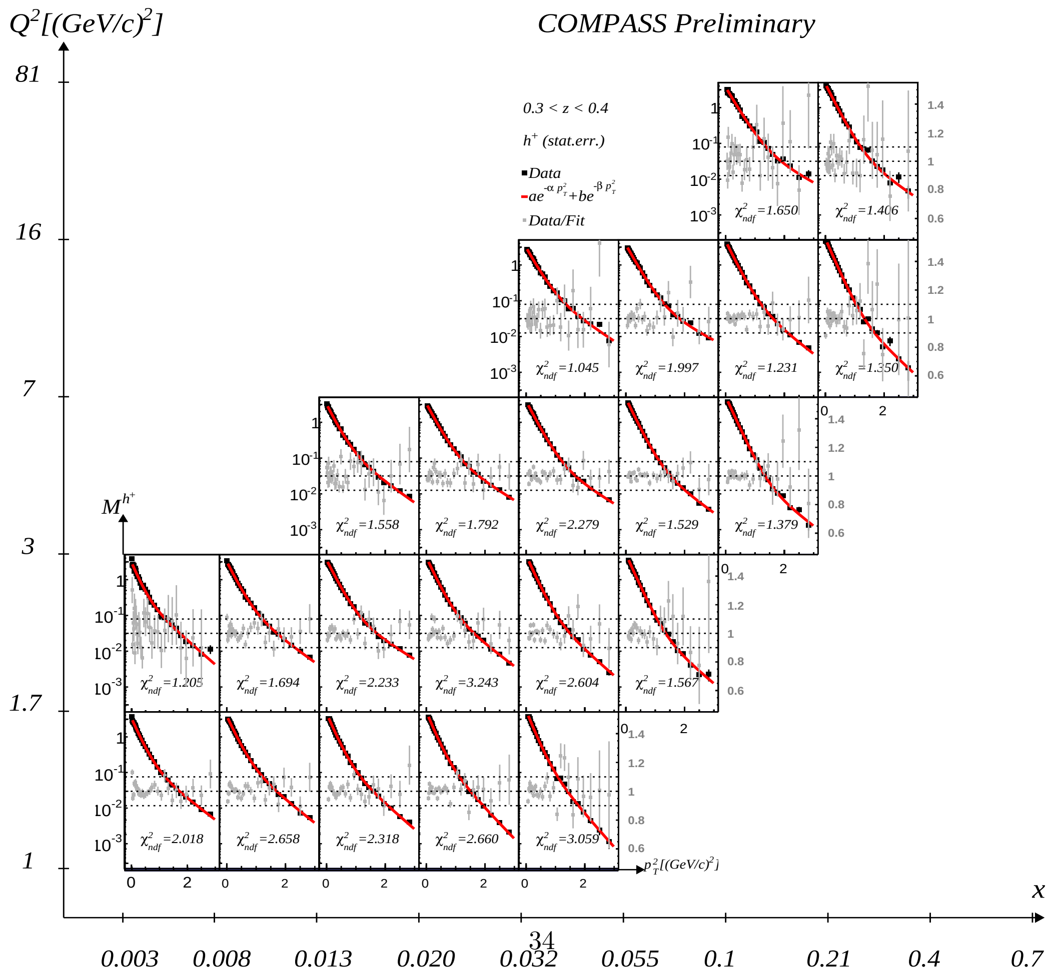

(b) negative hadrons

Figure 18: Differential p_T^2-dependent hadron multiplicities in different x, Q^2 and z bins fitted with two-exponentials function ($ae^{-\alpha p_T^2} + be^{-\beta p_T^2}$). Only statistical errors are shown and used in the fits.

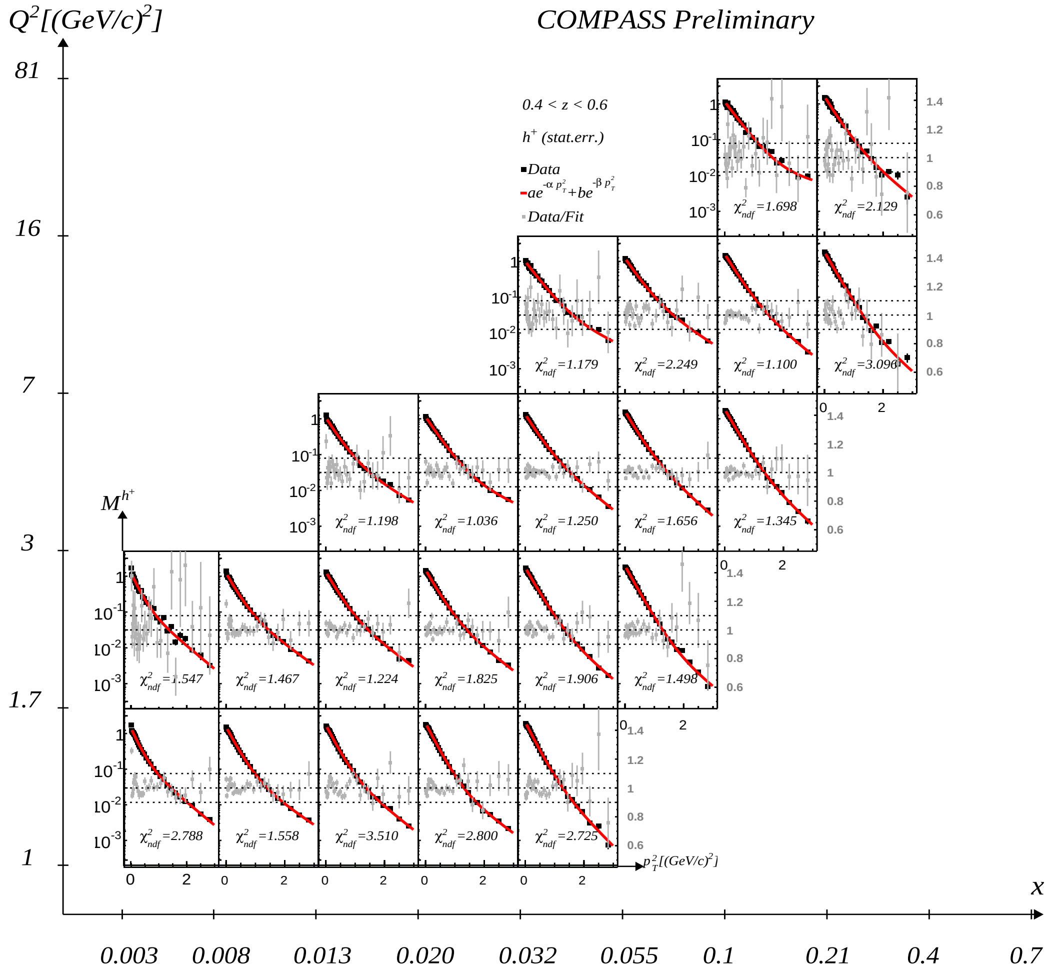

(a) positive hadrons

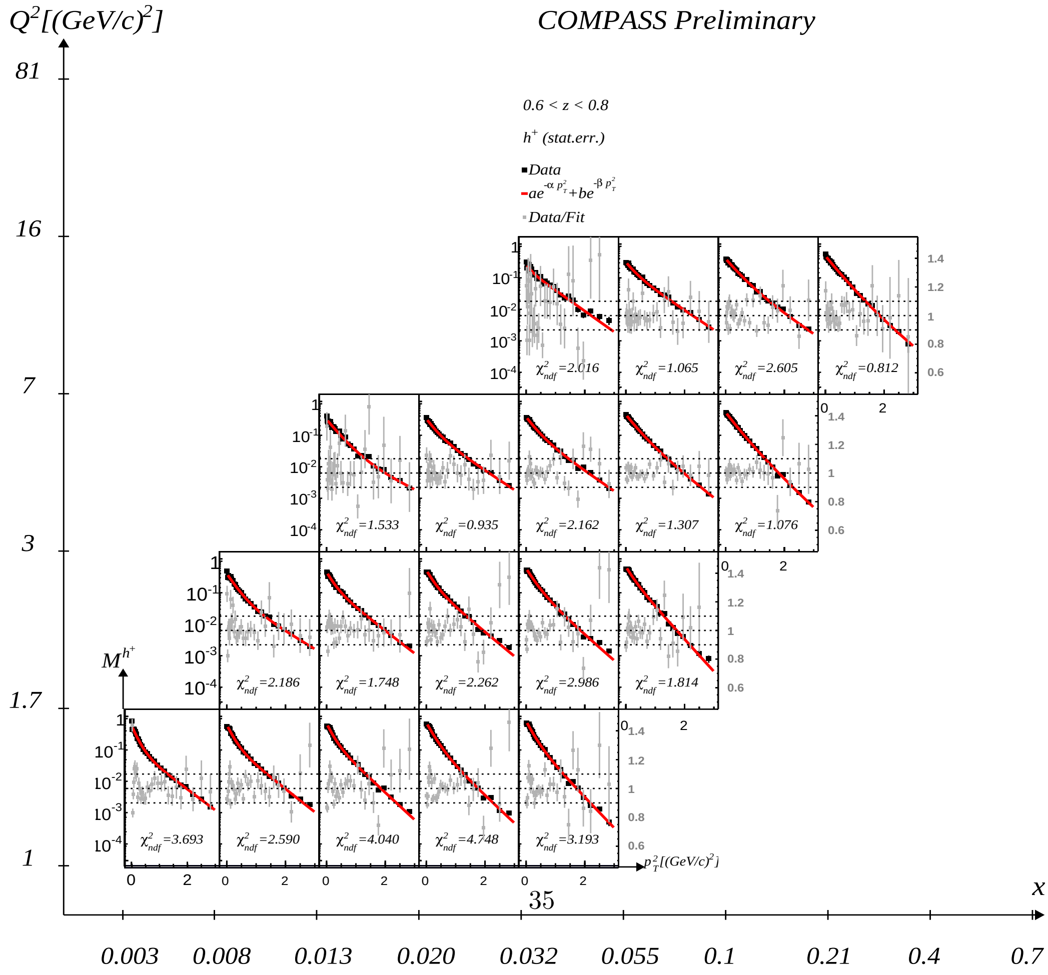

(b) negative hadrons

References

[1] M. Anselmino, M. Boglione, J. O. Gonzalez H., S. Melis and A. Prokudin, JHEP **1404**, 005 (2014)

[2] C. Adolph *et al.* [COMPASS Collaboration], Eur. Phys. J. C **73**, 2531 (2013)

[3] Jean-Francois Rajotte, PhD, Ludwig-Maximilians-Universität München, August 2010.

[4] N. Makke *et al.*, "Extraction of transverse momentum dependent distributions from 2006 data for unidentified hadrons", Release Note, June 2014

[5] G. Sbrizzai, " $x - Q^2$ binning studies for the multi dimensional analysis of the 2010 transverse data", talk at Transversity meeting, April 17, 2014

[6] N. Makke, Talk at Analysis Meeting, September 2014

[7] I. Savin, Azimuthal asymmetries from 2006 data, Analysis Meeting, August 2012

[8] MC option files
∼ybedfer/geant.utils/lepto.MSTW08.psON.opt,v1.1 and geant.FLUKA.2006.opt,v1.1

[9] M. Stolarski et al., Gluon polarisation from high P_T hadron pair events, release Note, September 2010

[10] T. Ullrich and Z. Xu, arXiv:physics/0701199, 2007

[11] F. Thibaud, Talk at Analysis Meeting, March 2013

[12] N. Makke *et al.*, Release Note on pion and kaon multiplicities from 2006 data, April 2013

[13] B. Badelek, D. Bardin, K. Kurek and K. Scholz, Z. Phys. C 66 (1995) 591

[14] N. Makke, Talk at Analysis Meeting, December 2014

[15] http://wwwcompass.cern.ch/compass/software/offline/input/radcor/

[16] N. Makke *et al.*, talk at COMPASS analysis meeting, May 2014.

[17] Discussion in SIDIS subgroup.

[18] N. Makke, talk at COMPASS analysis meeting, September 2013.